J|A|C|S
ARTICLES
Published on Web 03/11/2005

Exciton Migration in Rigid-Rod Conjugated Polymers: An Improved Förster Model

Emmanuelle Hennebicq,[†,‡] Geoffrey Pourtois,[†] Gregory D. Scholes,[§] Laura M. Herz,[||,#] David M. Russell,[||] Carlos Silva,[||] Sepas Setayesh,[⊥] Andrew C. Grimsdale,[⊥] Klaus Müllen,[⊥] Jean-Luc Brédas,[†,‡] and David Beljonne*[,†,‡]

Contribution from the Chemistry of Novel Materials, University of Mons-Hainaut, Place du Parc 20, B-7000 Mons, Belgium, School of Chemistry and Biochemistry, Georgia Institute of Technology, 770 State Street, Atlanta, Georgia 30332-0400, Lash Miller, Chemical Laboratories, University of Toronto, 80 Saint George Street, Toronto, Ontario, Canada M5S 3H6, Cavendish Laboratory, University of Cambridge, Madingley Road, Cambridge CB3 0HE, United Kingdom, and Max-Planck-Institute for Polymer Research, Ackermannweg 10, D-55128, Mainz, Germany

Received February 27, 2004; E-mail: David@averell.umh.ac.be

Abstract: The dynamics of *interchain* and *intrachain* excitation energy transfer taking place in a polyindenofluorene endcapped with perylene derivatives is explored by means of ultrafast spectroscopy combined with correlated quantum-chemical calculations. The experimental data indicate faster exciton migration in films with respect to solution as a result of the emergence of efficient channels involving hopping between chains in close contact. These findings are supported by theoretical simulations based on an improved Förster model. Within this model, the rates are expressed according to the Fermi golden rule on the basis of (i) electronic couplings that take account of the detailed shape of the excited-state wave functions (through the use of a multicentric monopole expansion) and (ii) spectral overlap factors computed from the simulated acceptor absorption and donor emission spectra with explicit coupling to vibrations (considered within a displaced harmonic oscillator model); inhomogeneity is taken into account by assuming a distribution of chromophores with different conjugation lengths. The calculations predict faster *intermolecular* energy transfer as a result of larger electronic matrix elements and suggest a two-step mechanism for *intrachain* energy transfer with exciton hopping along the polymer backbone as the limiting step. Injecting the calculated hopping rates into a set of master equations allows the modeling of the dynamics of exciton transport along the polyindenofluorene chains and yields ensemble-averaged energy-transfer rates in good agreement with experiment.

I. Introduction

Resonance energy transfer (RET) refers to a nonradiative photophysical process whereby an excited donor fluorophore "D" transfers its excitation energy to an acceptor chromophore "A"; thus, it can be viewed as a virtual photon exchange between two interacting molecules that arises from the coupling between the donor radiative decay and the excitation of the acceptor molecule. RET processes are involved in the mechanism of crucial biological processes such as light harvesting in photosynthetic systems.[1] The powerful machinery designed by Nature through evolution has inspired scientists to take advantage of ultrafast energy-transfer processes in the development of synthetic light-harvesting systems. Fast energy transfer is also essential to achieve efficient internal color conversion[2] in electroluminescent devices, to ensure excitation migration toward dissociation zones in solar cells,[3] or to promote delicate (bio)chemical sensing.[4−6] Energy transfer within assemblies of small organic molecules can also prove useful in the achievement of low-cost nanoscale photonic devices.[7−10]

[†] University of Mons-Hainaut.
[‡] Georgia Institute of Technology.
[§] University of Toronto.
[||] University of Cambridge.
[⊥] Max-Planck-Institute for Polymer Research.
[#] Current address: Clarendon Laboratory, University of Oxford, Parks Road, Oxford OX1 3PU, United Kingdom.

(1) Van Grondelle, R.; Dekker: J. P.; Gillbro, T.; Sundström, V. *Biochim. Biophys. Acta* **1994**, *1187*, 1; Sundström, V.; Pullerits, T.; Van Grondelle, R. *J. Phys. Chem. B* **1999**, *103*, 2327; Scholes, G. D.; Fleming, G. R. *J. Phys. Chem. B* **2000**, *104*, 1854; Shreve, A. P.; Trautman, J. K.; Frank, H. A.; Owens, T. G.; Albrecht, A. C. *Biochim. Biophys. Acta* **1991**, *1058*, 280; Jimenez, R.; Dikshit, S. N.; Bradforth, S. E.; Fleming, G. R. *J. Phys. Chem.* **1996**, *100*, 6925; Visser, H. M.; Kleima, F. J.; van Stokkum, I. H. M.; van Grondelle, R.; van Amerongen, H. *Chem. Phys.* **1996**, *210*, 297; Kleinekathofer, U.; Schulten, A. *Phys. Rev. E* **2002**, *65*, 031919.

(2) List, E. W. J.; Holzer, L.; Tasch, S.; Leising, G.; Scherf, U.; Müllen, K.; Catellani, M.; Luzzati, S. *Solid-State Commun.* **1999**, *109*, 455; Lee, J.-I.; Kang, I.-N.; Hwang, D.-H.; Shim, H.-K.; Jeoung, S. C.; Kim, D. *Chem. Mater.* **1996**, *8*, 1925; Wang, H.-L.; McBranch, D.; Klimov, V. I.; Helgerson, R.; Wudl, F. *Chem. Phys. Lett.* **1999**, *315*, 173.

(3) Halls, J. J.; Walsh, C. A.; Greenham, N. C.; Marseglia, E. A.; Friend, R. H.; Moratti, S. C.; Holmes, A. B. *Nature* **1995**, *376*, 498; Sariciftci, N. S.; Smilowitz, L.; Heeger, A. J.; Wudl, F. *Science* **1992**, *258*, 1474; Yu, G.; Gao, J.; Hummelen, J. C.; Wudl, F.; Heeger, A. J. *Science* **1995**, *270*, 1789.

(4) Chen, L.; McBranch, D. W.; Wang, H.-L.; Hegelson, R.; Wudl, F.; Whitten, D. G. *Proc. Natl. Acad. Sci. U.S.A.* **1999**, *96*, 12287.

(5) Jones, R. L.; Lu, L.; Hegelson, R.; Bergstedt, T. S.; McBranch, D.; Whitten, D. G. *Proc. Natl. Acad. Sci. U.S.A.* **2001**, *98*, 14769; Swager, T. M.; Wosnick, J. H. *MRS Bull.* **2002**, *27*, 446; Wang, D.; Gong, X.; Heeger, P. S.; Rininsland, F.; Bazan, G. C.; Heeger, A. J. *Proc. Natl. Acad. Sci. U.S.A.* **2002**, *99*, 49; Stork, M.; Gaylord, B. S.; Heeger, A. J.; Bazan, G. C. *Adv. Mater.* **2002**, *14*, 361.

(6) Zhou, Q.; Swager, T. M. *J. Am. Chem. Soc.* **1995**, *117*, 12593; McQuade, D. T.; Pullen, A. E.; Swager, T. M. *Chem. Rev.* **2000**, *100*, 2537; McQuade, D. T.; Hegedus, A. H.; Swager, T. M. *J. Am. Chem. Soc.* **2000**, *122*, 12389.

10.1021/ja0488784 CCC: $30.25

These results have triggered a tremendous interest in developing a detailed understanding, at the microscopic level, of the fundamental mechanisms underlying excitation energy-transfer phenomena in conjugated materials. This interest has been fueled by the need to control the energy flow in organic materials, which strongly impacts the resulting device efficiencies. For instance, a strong red shift in emission wavelength upon excitation has been reported for polyfluorene-based electroluminescent diodes as a result of photo- or electro-oxidation; the modifications of the optical properties have been assigned to the presence of lower band-gap fluorenone chromophores that act as traps for the excitation energy.[11]

The link between exciton dynamics and microscopic organization of the chromophores needs to be better understood to enable the design of elaborate systems, wherein for instance, the transfer process toward the molecular targets with the desired optical features is favored and exciton trapping on low-lying defects is minimized. One of the main issues in setting up such a microscopic model concerns the relative efficiencies of *interchain* versus *intrachain* energy-transfer processes. We note that here *intrachain* energy migration refers to motion along the conjugated backbone of a single polymer chain in the absence of any chain-to-chain contact (rigid-rod structure), while *interchain* transfer refers to a through-space energy process between closely spaced chromophores (either belonging to different polymer chains or brought close to one another as a result of chain folding). It has been demonstrated by Schwartz and co-workers[12] that in alkoxy-substituted poly(*p*-phenylene vinylene) the exciton diffusion is slowed when *interchain* interactions are inhibited due to incorporation of single conjugated chains in the pores of a silica matrix. Less effective *intrachain* energy migration compared to *interchain* transfer has been attributed to weak dipole coupling of the excitations along the chain direction.[12,13]

In this work, we investigate both *intramolecular* and *intermolecular* energy-transfer processes in a covalently linked donor−acceptor pair, namely, a polyindenofluorene (PIF) strand endcapped with red-emitting perylene monoimide derivatives. The system under investigation is α,ω-bis(*N*-(2,6-diisopropylphenyl)-1,6-bis-(4-*tert*-butylphenoxy)-3,4-dicarbonicacidimide-9-perylene-poly-2,8-(6,6,12,12-tetraethylhexyl)indenofluorene, hereafter abbreviated PEC-PIFTEH (the chemical structure is displayed in Figure 1).

In such a system, light absorption by the polymer bridge is followed by migration of the resulting electronic excitations toward the lower optical gap perylene derivatives acting as

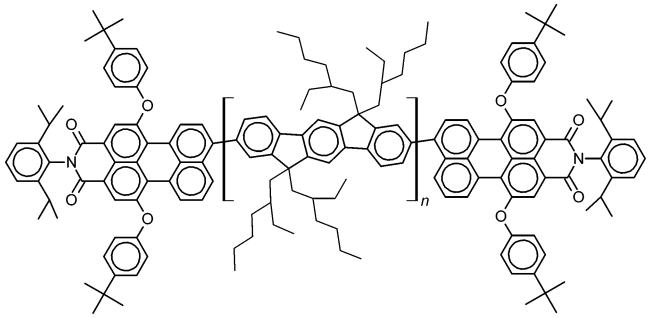

Figure 1. Molecular structure of α,ω-bis(*N*-(2,6-diisopropylphenyl)-1,6-bis-(4-*tert*-butylphenoxy)-3,4-dicarbonicacidimide-9-perylene-poly-2,8-(6,6,-12,12-tetraethylhexyl)indenofluorene (PEC-PIFTEH).

exciton traps. Energetic disorder together with strong electron−phonon coupling, which are typical characteristics of most conjugated polymers, lead to localization of the excitation energy over individual conformational subunits. The polymer chains can then be regarded as made from a statistical distribution of segments with different conjugation lengths and hence different excitation energies. Energy migration proceeds incoherently through a sequence of hopping events between the localized sites that contribute to the density of states (DOS) on an energy scale.[14] Upon photoexcitation, unidirectional long-range exciton hopping along the polyindenofluorene chains from high-energy short conjugated segments toward lower-energy sites takes place prior to energy transfer to the perylene endcaps. Dispersive relaxation of the photoexcitations through incoherent hopping among localized states has also been reported in thin films of poly(fluorene),[15] which is a member of the same ladder-type poly(*p*-phenylene) family as PIF.

In solution, direct interactions between the perylene endcaps and the conjugated segments can be ruled out when considering that the rigid-rodlike structure of the PIF chains prevents any chain folding (in contrast to the situation encountered in PPV derivatives);[16] incoherent exciton hopping *along the PIF chains* is therefore expected to be the main exciton migration channel. In the solid state, additional pathways for energy migration open up, such as direct *interchain* transfer from a photoexcited indenofluorene segment to a closely located perylene derivative attached to a neighboring chain.

In this work, exciton dynamics in PEC-PIFTEH is investigated by combining time-resolved spectroscopy measurements and correlated quantum-chemical calculations. The experimental results are interpreted in the framework of a theoretical approach based on an improved Förster model,[17,18] wherein the electronic matrix elements for energy transfer are calculated from a multicentric monopolar representation of the transition dipole moments (atomic transition densities).[19] The elementary steps involved in *intrachain* and *interchain* energy migration have been modeled first. The results suggest that in this polymer intramolecular energy hopping rates are small with respect to

(7) Rispens, M. T.; Sanchez, L.; Knol, J.; Hummelen, J. C. *Chem. Commun.* **2001**, *163*; Sanchez, L.; Rispens, M. T.; Hummelen, J. C. *Angew. Chem.* **2002**, *41*, 838.
(8) El-Ghayoury, A.; Schenning, A. P. H. J.; Van Hal, P. A.; Van Duren, J. K. J.; Janssen, R. A. J.; Meijer, E. W. *Angew. Chem.* **2001**, *40*, 3660.
(9) El-Ghayoury, A.; Peeters, E.; Schenning, A. P. H. J.; Meijer, E. W. *Chem. Commun.* **2000**, *19*, 1969; Schenning, A. P. H. J.; Jonkheijm, P.; Peeters, E.; Meijer, E. W. *J. Am. Chem. Soc.* **2001**, *123*, 409; Beckers, E. H. A.; Van Hal, P. A.; Schenning, A. P. H. J. *J. Mater. Chem.* **2002**, *12*, 2054.
(10) Herz, L. M.; Daniel, C.; Silva, C.; Hoeben, F. J. M.; Schenning, A. P. H. J.; Meijer, E. W.; Friend, R. H.; Phillips, R. T. *Phys. Rev. B* **2003**, *68*, 045203.
(11) Scherf, U.; List, E. J. W. *Adv. Mater.* **2002**, *14*, 477; Zojer, E.; Potgansch, A.; Hennebicq, E.; Beljonne, D.; Brédas, J.-L.; Scandiucci de Freitas, P.; Scherf, U.; List, E. J. W. *J. Chem. Phys.* **2002**, *17*, 6794.
(12) Nguyen, T. Q.; Wu, J.; Doan, V.; Schwartz, B. J.; Tolbert, S. H. *Science* **2000**, *288*, 652; Nguyen, T. Q.; Wu, J.; Tolbert, S. H.; Schwartz, B. J. *Adv. Mater.* **2001**, *13*, 609.
(13) Wang, C. F.; White, J. D.; Lim, T. L.; Hsu, J. H.; Yang, S. C.; Fann, W. S.; Peng, K. Y.; Chan, S. A. *Phys. Rev. B* **2003**, *67*, 035202.
(14) Pauck, T.; Bässler, H.; Grimme J.; Scherf, U.; Müllen, K. *Chem. Phys.* **1996**, *210*, 219.
(15) Meskers, S. C. J.; Hübner, J.; Oestereich, M.; Bässler, H. *J. Phys. Chem. B* **2001**, *105*, 9139.
(16) Yu, J.; Hu, D.; Barbara, P. F. *Science* **2000**, *289*, 1327.
(17) Förster, T. *Ann. Phys.* **1948**, *2*, 55; Förster, T. *Discuss. Faraday Soc.* **1959**, *27*, 7; Förster, T. *Pure Appl. Chem.* **1970**, 24, 443; Förster, T.; Kasper, K. *Z. Elektrochem.* **1955**, *59*, 976.
(18) Van der Meer, B. W.; Coker, G. I.; Chen-y, S. *Resonance Energy Transfer, Theory and Data*; Wiley: New York, 1994.
(19) Marguet, S.; Markovitsi, D.; Millié, P.; Sigal, H.; Kumar, S. *J. Phys. Chem. B* **1998**, *102*, 4697.

the corresponding intermolecular values, a picture that is consistent with the measured exciton dynamics in solution compared to that in films. In a second step, long-range intramolecular energy motion along the PIF chains as well as trapping dynamics are investigated by means of a Pauli master equation (PME) approach,[20] wherein excitation migration occurs through a random walk among localized conformational subunits. Excitation diffusion along the polymer chains is found to compete with radiative decay, in good agreement with the experimental data in solution.

II. Theoretical Background and Methodology

Hopping Rates. Depending on the relative magnitude of the electronic coupling promoting the energy-transfer process between donor and acceptor, V_{DA}, and the donor vibrational relaxation energy, E_{rel}^{D}, two limiting cases can be distinguished for energy transfer, which are referred to as the weak and strong coupling mechanisms. In the weak coupling regime, interchromophore electronic interaction is assumed to be (much) smaller than the vibrational reorganization energy ($V_{DA} \ll E_{rel}^{D}$), which implies that an excited chromophore relaxes to its equilibrium geometry prior to hopping to a neighboring molecule. In this regime, energy migration takes place through sequential incoherent hopping steps between localized chromophores (nonadiabatic limit); the excitation motion can be described as Markovian, each elementary transfer step being independent of the history of the overall excitation migration process. In contrast, in the strong coupling limit ($V_{DA} \gg E_{rel}^{D}$), vibrational motion occurs on a much longer time scale than electronic motion, and the excitation wave functions spread over the whole system without any self-localization (adiabatic limit). Recent joint experimental and theoretical studies performed on phenylacetylene dendrimers suggest that these molecules, in their relaxed excited-state geometries, actually belong to the strong coupling regime as a result of contributions from through-bond charge-transfer excitations.[21]

In the system we investigate, the magnitude of the electronic coupling between neighboring chromophores is calculated to be smaller than the geometric relaxation on an isolated chromophore. Therefore, the energy-transfer processes can be reasonably modeled in the framework of the weak coupling regime and a Förster-like approach. Within this model, the rate for energy transfer between an excited donor and a ground-state acceptor, k_{DA}, can be derived from time-dependent perturbation theory and the Fermi golden rule as:[20,22−23]

$$k_{DA} = \frac{2\pi}{\hbar} |V_{DA}|^2 \,(\mathrm{FCWD}) \qquad (1)$$

where V_{DA} is the electronic matrix element for energy transfer, which can be viewed as a measure of the electronic interaction between excitations localized over the donor and acceptor moieties; FCWD stands for the Franck−Condon weighted density-of-states factor, corresponding to the product of the density of vibrational states in the initial and final states and their spectral overlap. It can be recast in terms of the overlap between donor emission and acceptor absorption spectra normalized on an energy scale as (see Supporting Information):

$$k_{DA} = 1.18|V_{DA}|^2 \int_0^\infty \mathrm{d}E\, F_D(E) A_A(E) = 1.18|V_{DA}|^2 J_{DA} \qquad (2)$$

where $F_D(E)$ and $A_A(E)$ denote the donor fluorescence and acceptor absorption spectra, respectively, normalized on a cm^{-1} scale; in eq 2, the electronic matrix element is expressed in cm^{-1} and the transfer rate in ps^{-1}.

Electronic Couplings. The tunneling matrix element, V_{DA}, involves the unperturbed (zero-order) initial and final wave functions, given by a simple product of the localized excited-state donor (ψ_{D^*}) and ground-state acceptor (ψ_A) wave functions and vice versa, respectively:

$$V_{DA} = \langle \psi_i^o | H_{DA} | \psi_f^o \rangle = \langle \psi_{D^*} \psi_A | H_{DA} | \psi_D \psi_{A^*} \rangle \qquad (3)$$

where H_{DA} is the perturbation describing the donor−acceptor interaction. Within the single configuration interaction (SCI) approach adopted here, the donor ground-state and excited-state wave functions write (similar expressions can be obtained for the acceptor):

$$|\psi_D\rangle = |HF_D\rangle\,;\; |\psi_{D^*}\rangle = \sum_{i\to a}^{D} Z_{i\to a} (a_{D\uparrow}^{+} i_{D\uparrow} + a_{D\downarrow}^{+} i_{D\downarrow}) |HF_D\rangle \qquad (4)$$

where $|HF_D\rangle$ denotes the Hartree−Fock self-consistent-field ground-state determinant, $a_{D\uparrow}^{+}$ [$i_{D\uparrow}$] creates an electron with spin up on unoccupied molecular orbital (MO) a [removes an electron with spin up on occupied MO i] and $Z_{i\to a}$ is the CI expansion coefficient associated with the $i\to a$ single excitation. Injecting eq 4 into eq 3 leads to:

$$V_{DA} = \sum_{i,a}^{D} \sum_{j,b}^{A} Z_{i\to a}^{D} Z_{j\to b}^{A} \{2[b_A j_A | a_D i_D] - [b_A i_D | a_D j_A]\} - P = 2J - K - P \qquad (5)$$

which involves two-electron Coulombic contributions:

$$J = [b_A j_A | a_D i_D] = \frac{1}{4\pi\epsilon_0} \int \mathrm{d}r_1 \mathrm{d}r_2 b_A^*(r_1) j_A(r_1) \frac{1}{r_{12}} a_D^*(r_2) i_D(r_2)$$

and exchange contributions:

$$K = [b_A i_D | a_D j_A] = \frac{1}{4\pi\epsilon_0} \int \mathrm{d}r_1 \mathrm{d}r_2 b_A^*(r_1) i_D(r_1) \frac{1}{r_{12}} a_D^*(r_2) j_A(r_2)$$

P encompasses the remaining (penetration) terms that depend explicitly on the overlap between donor and acceptor molecular orbitals.[24]

Energy transfer promoted by Coulombic interactions, referred to as the Förster mechanism, is a long-range process whose efficiency is directly related to the dipole strength of the donor and acceptor electronic transitions. In contrast, energy-transfer processes via exchange interactions (Dexter mechanism)[25] or orbital penetration are short-range processes, which scale as the overlap between the donor and acceptor orbitals (i.e., decay exponentially with distance). Exchange contributions only

(20) May, V.; Kühn, O. *Charge and Energy Transfer Dynamics in Molecular Systems*; Wiley: Berlin, 2000.
(21) Thompson, A. L.; Gaab, K. M.; Xu, J.; Bardeen, C. J.; Martinez, T. J. *J. Phys. Chem. A* **2004**, *108*, 671.
(22) Schatz, G. C.; Ratner, M. A. *Quantum Mechanics in Chemistry*; Prentice Hall: Englewood Cliffs, NJ, 1993.
(23) Scholes, G. D. *Annu. Rev. Phys. Chem.* **2003**, *54*, 57.
(24) Harcourt, R. D.; Scholes, G. D.; Ghiggino, K. P. *J. Chem. Phys.* **1994**, *101*, 10521.
(25) Dexter, D. L. *J. Chem. Phys.* **1953**, *21*, 836.

prevail when the electronic excitations involved in the RET process are optically forbidden or weakly allowed; these have not been accounted for here, and eq 5 then takes the simple form:

$$V_{\mathrm{DA}} = 2\sum_{i,a}^{\mathrm{D}}\sum_{j,b}^{\mathrm{A}} Z^{\mathrm{D}}_{i\to a}\, Z^{\mathrm{A}}_{j\to b}[b_{\mathrm{A}} j_{\mathrm{A}} | a_{\mathrm{D}} i_{\mathrm{D}}] \tag{6}$$

In the original Förster model, V_{DA} is further simplified by expanding eq 6 as a multipole expansion with respect to the center-to-center distance, which is truncated after the dipolar term:

$$V_{\mathrm{DA}} = \frac{\kappa}{4\pi\epsilon_0}\left(\frac{\mu_{\mathrm{D}}\,\mu_{\mathrm{A}}}{R^3_{\mathrm{DA}}}\right) \tag{7}$$

where μ_D and μ_A denote the magnitude of the donor and acceptor transition dipole moments (associated to the lowest optical excitation), respectively; R_{DA} is the center-to-center donor−acceptor interdistance; κ is a factor depending on the relative orientations of the dipoles:

$$\kappa = \vec{\mu}_{\mathrm{D}}\,\vec{\mu}_{\mathrm{A}} - 3(\vec{\mu}_{\mathrm{D}}\,\vec{\mathrm{u}}_{\mathrm{DA}})(\vec{\mu}_{\mathrm{A}}\,\vec{\mathrm{u}}_{\mathrm{DA}}) \tag{8}$$

where $\vec{\mu}_{\mathrm{DA}}$ is the unit vector connecting the centers of the donor and acceptor, $\vec{\mu}_{\mathrm{D}}$ and $\vec{\mu}_{\mathrm{A}}$ are unit vectors defining the orientation of transition moments for the donor and the acceptor. Such an approach averages away the shapes of the donor and acceptor wave functions and should only be applied when the size of the interacting molecules is small with respect to the intermolecular separation. This is hardly the case in polymeric materials where the point-dipole model (PDM) is expected to break down. To account for the detailed chemical structure and topology of the interacting chromophores, we have adopted an "improved" Förster formalism, wherein the total electronic coupling is expressed as a sum over pairwise interactions between atomic transition charges (as obtained by expanding eq 6 in a zero-differential-overlap (ZDO) approximation):[26]

$$\begin{aligned} V^{\mathrm{Coul}}_{\mathrm{DA}} &= 2\sum_{i,a}^{\mathrm{D}}\sum_{j,b}^{\mathrm{A}}\sum_{p}^{\mathrm{D}}\sum_{q}^{\mathrm{A}} Z^{\mathrm{D}}_{i\to a}\, Z^{\mathrm{A}}_{j\to b} C_{ip} C_{ap} C_{jq} C_{bq} [\chi_p \chi_p | \chi_q \chi_q] \\ &= \frac{1}{4\pi\epsilon_0}\sum_{p}^{\mathrm{D}}\sum_{q}^{\mathrm{A}} \frac{\rho_{\mathrm{D}}(p)\rho_{\mathrm{A}}(q)}{r_{pq}} \end{aligned} \tag{9}$$

where the summation runs over all sites $p[q]$ on the donor [acceptor]; r_{pq} denotes the distance between atomic centers p and q; χ_p and $\chi_q$correspond to atomic orbitals on sites p and q; $C_{ip}$is the LCAO coefficient for MO i on site p; $\rho_D(p)[\rho_A(q)]$ is the atomic transition density on site $p[q]$ calculated for the lowest optical excitation on the donor (acceptor):

$$\rho_{\mathrm{D}}(p) = \sqrt{2}\sum_{i,a}^{\mathrm{D}} Z^{\mathrm{D}}_{i\to a} C_{ip} C_{ap}\ [\rho_{\mathrm{A}}(q) = \sqrt{2}\sum_{j,b}^{\mathrm{D}} Z^{\mathrm{A}}_{j\to b} C_{jq} C_{bq}] \tag{10}$$

The transition densities provide a local map of the electronic transition dipole moment, with (for the x-component of the donor transition dipole):

$$\mu^{x}_{\mathrm{D}} = \sum_{m} \rho_{\mathrm{D}}(m)\, x_m \tag{11}$$

with x_m the x-coordinate for site m.

Spectral Overlap Factors. Conjugated systems are usually characterized by strong electron-vibration coupling. The correlation between electronic and vibrational degrees of freedom leads to electronic and nuclear reorganizations upon photoexcitation and the appearance of a vibronic progression in the absorption and emission spectra. In the Franck−Condon picture, coupling between electronic and vibrational transitions implies a displacement of the ground and excited equilibrium geometries relative to each other along some normal coordinates (which are said to be coupled to the electronic transition). As a result of strong electron-vibration coupling, the spectral intensity is obtained as a superposition of transitions between the manifold of vibration states (of the coupled normal modes) associated to the ground and excited state. To compute the spectral overlap factors in eq 2, absorption and emission spectra have been simulated within the approximation of undistorted displaced harmonic oscillators. The ground-state and excited-state potential energy curves are thus described by parabolas with identical curvatures and displaced with respect to one another along the relevant normal vibration modes.

In the hypothetical case of quadratic potential energy surfaces displaced along one single normal mode, the shape of a vibrational progression at 0 K follows a simple Poisson distribution:[27−29]

$$I_{0-n}(\nu) \propto F^2_{0-n}(\nu) = \frac{(S_\nu)^n\, \mathrm{e}^{-S}{}_\nu}{n!} \tag{12}$$

where $F^2_{0-n}(\nu)$ denotes the Franck−Condon factor for mode n, defined as the squared overlap integral between the vibrational ground-state level of the initial electronic state and the nth thvibrational excited-state level of the final electronic state; S_n, the Huang−Rhys factor associated to the nth active mode, is a measure of the electron-vibration coupling and corresponds to the ratio of the nuclear reorganization energy along the normal coordinate, λ_ν, and the corresponding vibrational energy $\hbar\omega_\nu$:[27−31]

$$S_\nu = \frac{\lambda_\nu}{\hbar\omega_\nu} = \frac{f}{2\hbar\omega_\nu}(\Delta Q_{\mathrm{el},\nu})^2 \tag{13}$$

where $\mathrm{D}Q_{\mathrm{el},\nu}$ is the change in equilibrium geometry between the ground state and the excited state along the nth normal coordinate and f is the corresponding force constant. Equation 12 can be readily extended as a product of Franck−Condon factors associated to all normal modes coupled to the excitation. In addition, when kT is comparable to $\hbar\omega_\nu$(which is the case

(26) When based on ab initio electronic structure calculations, the electronic coupling involves interactions between the full three-dimensional wave functions (transition density cubes). See: Krueger, B. P.; Scholes, G. D.; Fleming, G. R. *J. Phys. Chem. B* **2000**, *104*, 1854.
(27) Lax, M. *J. Chem. Phys.* **1952**, *20*, 1752; Keil, T. H. *Phys. Rev.* **1965**, *140*, 601; Di Bartolo, B.; Powell, R. C. *Phonons and Resonances in Solids*; Wiley: New York, 1975.
(28) Gierschner, J.; Mack, H.-G.; Lüer, L.; Oelkrug, D. *J. Chem. Phys.* **2002**, *116*, 8596.
(29) Karaburnaliev, S.; Bittner, E.; Baumgarten, M. *J. Chem. Phys.* **2001**, *114*, 5863.
(30) Cornil, J.; Beljonne, D.; Heller, C.-M.; Campbell, I.-H.; Laurich, B.; Smith, D.; Brédas, J.-L. *Chem. Phys. Lett.* **1997**, *278*, 139.
(31) Cornil, J.; Beljonne, D.; Brédas, J.-L. *J. Chem. Phys.* **1995**, *103*, 834.

for librational modes at room temperature), excited vibrational levels are populated and the spectra are simulated by considering a Boltzmann distribution of vibrational quanta (eq 12 needs then to be rewritten by considering all possible transitions between vibrational levels m and n in the initial and final states).[32] Since a complete Franck−Condon treatment of all the coupled vibrational modes is too computationally demanding, only the normal vibrational modes with the largest Huang−Rhys factors are generally considered in the simulations of optical spectra.

Spectra of extended π-conjugated systems such as poly(*p*-phenylenevinylene), poly(*p*-phenylene), and the corresponding ladder-type systems (which include polyindenofluorenes) are generally dominated by a vibronic progression originating from the coupling to high-frequency C═C stretching modes lying in the energy range between 1200 and 1600 cm^{-1}.[28−36] In addition, nonnegligible coupling to low-frequency ring-torsional modes has been reported for floppy molecules presenting torsional degrees of freedom; this is the case for poly(*p*-phenylene) and poly(indenofluorene). It has been demonstrated that relaxation in torsional degrees of freedom for these molecules covers a large fraction (in the range of 80%) of the mass-weighted interstate distortion on going from ground-state to excited-state geometries.[29] The large displacement of Born−Oppenheimer potential surfaces on going from the ground to the excited electronic state is consistent with the strong coupling of these low-frequency modes to the electronic transition.

Direct comparison of experimental spectra and theoretical studies based on the use of quantum-chemical techniques, showed that coupling to these low-frequency modes affects strongly the band shapes of the absorption and emission spectra. The vibronic bands associated to these modes cannot be resolved in inhomogeneously broadened spectra as a result of the small energy separation between the vibrational sublevels (typically less than 100 cm^{-1}) but lead to a broadening of the absorption features and the lack of mirror symmetry between emission and absorption at room temperature.[33] The very large Huang−Rhys factor associated to the torsion modes, on the order of 10 for poly(*p*-phenylene) compounds, leads to a vibronic progression with a Gaussian-like shape. Including these low-frequency modes opens up a Stokes shift between the apparent 0−0 lines (the absorption spectrum being blue-shifted while the emission spectrum is shifted to the red), as described by Karaburnaliev and Bittner,[29] and leads to a temperature-dependent broadening of the vibrational features. As a result of this Stokes shift, the spectral overlap between absorption and emission spectra is significantly reduced. It is thus important to consider the coupling of the low-frequency libration modes to the electronic excitations when computing the spectral overlap factors.

In our simulations, spectral overlap factors were calculated on the basis of acceptor absorption and donor emission spectra (normalized on an energy scale) simulated within the Franck−Condon approximation by considering two main effective vibrational modes:

(i) a high-frequency mode (at 1300 cm^{-1}) representative of the dominant carbon−carbon stretching and ring breathing vibrational motions in phenylene-based conjugated polymers;

(ii) a low-frequency libration mode (at 80 cm^{-1}).

The effective frequency associated to the C═C stretching modes considered here has been derived from the mean energy spacing between the main vibronic bands of the experimental spectra, while the frequency associated to the ring-torsional motions is the theoretical value obtained by Karaburnaliev and Bittner[29] for oligo(*p*-phenylene)s.

The Huang−Rhys factors associated to the high-frequency vibrational mode have been extracted from the calculated relaxation energies (at the INDO/SCI level) while constraining the molecule to a planar conformation (thus, freezing out the torsional motions to disentangle the contributions to the relaxation energy associated to the two types of motion). The Huang−Rhys factors for the low-frequency mode have been adjusted to fit the Stokes shifts measured in oligomer solutions at room temperature: $S \approx 14$ was found to lead to the best agreement with experiment. Note that this value is higher than that reported for the libration mode in oligophenylenes;[29] one should thus regard this vibration mode as an effective mode accounting for all low-frequency vibrations coupled to the excitation (i.e., libration as well as soft acoustic modes or *intermolecular* modes[37]). Such an effective mode thus also encompasses modes associated with the bath (solvent), which can be typically modeled as Brownian oscillators. However, a simplified model can also be employed that contains a discrete number of modes, or even just a single mode, and provides a phenomenological description of the line broadening. In that case the bath spectral density is represented by, for example, one average frequency. Linear spectroscopies, such as absorption and fluorescence, in the high temperature limit are generally insensitive to the precise model used to construct the homogeneous line broadening, so for the present purposes we employ the simplest model of a single average bath frequency to model the bath fluctuations. The low-frequency effective mode is thus expected to properly account for solvation effects. Note also that the use of undistorted harmonic potentials for the treatment of ring-torsional vibration modes represents a rather crude approximation and that a more sophisticated study accounting for the exact shape of the potentials would be more appropriate.[33] These are, however, currently out of reach for the long oligomers investigated here. Nevertheless, we stress that our simple model allows us to reproduce the overall shapes of the absorption and emission spectra and to assess the influence of coupling to low-frequency modes on the optical properties. In addition, we find that it provides a reasonable description of the spectral overlap factors, when compared to the values measured in oligomer solutions.

(32) Beljonne, D.; Brédas, J.-L.; Cha, M.; Torruellas W. E.; Stegeman, G. I.; Hofstraat J. W.; Horsthuis, H. H. G.; Möhlman, G. R. *J. Chem. Phys.* **1995**, *103*, 7834.

(33) Heimel, G.; Daghofer, M.; Von der Linden, W.; List, E. J. W.; Grimsdale, A. C.; Müllen, K.; Beljonne, D.; Brédas, J. L.; Zojer, E. *J. Chem. Phys.* In press.

(34) Tian, B.; Zerbi, G.; Schenk, R.; Müllen, K. *J. Chem. Phys.* **1995**, *95*, 3191; Chiavarone, L.; Terlizzi, M. D.; Scamarcio, G.; Babudri, F. G.; Farinola, M.; Naso F. *Appl. Phys. Lett.* **1999**, *75*, 2053; Ripamonti, E. A.; Very, J.; Dulieu, B.; Faulques, E.; Lefrant, S. *Synth. Met.* **1999**, *101*, 196; Gierschner, J.; Mack, H.-G.; Lüer, L.; Oelkrug, D. *J. Chem. Phys.* **2002**, *116*, 8596; Peeters, E.; Ramos, A. M.; Meskers, S. C. J.; Janssen, R. A. J. *J. Chem. Phys.* **2000**, *112*, 9445.

(35) Leising, G.; Verdon, T.; Louarn, G.; Lefrant, S. *Synth. Met.* **1991**, *41−43*, 279; Nijegorodov, N. I.; Downey, W. S.; Danailov, M. B. *Spectrochim. Acta, Part A* **2000**, 56, 783; Bredas, J.-L.; Cornil, J.; Heeger, A. J. *Adv. Mater.* **1996**, *8*, 447.

(36) Miller, E. K.; Maskel, G. S.; Yang, C. Y.; Heeger, A. *J. Phys. Rev. B* **1999**, *60*, 8028; Cadby, A. J.; Lane, P. A.; Mellor, H. S.; Martin, J.; Grell, M.; Giebler, C.; Bradley, D. D. C.; Wohlgenannt, M.; An, C.; Vardeny, Z. V. *Phys. Rev. B* **2000**, *62*, 15604; Ariu, M.; Lidzey, D. G.; Sims, M.; Cadby, A. J.; Lane, P. A.; Bradley, D. D. C. *J. Phys. Condens. Matter* **2002**, *14*, 9975; Scherf, U.; List, E. J. W. *Adv. Mater.* **2002**, *14*, 477.

(37) Johnston, M.B.; Herz, L. M.; Khan, A. L. T.; Köhler, A.; Davies, A. G.; Linfield, E. H. *Chem. Phys. Lett.* **2003**, *377*, 256.

The absorption and emission spectra have been convoluted by means of Lorentzian functions with an effective full width at half-maximum of 0.04 eV at room temperature to account for homogeneous broadening (fitted against the experimental oligomer spectra).

Long-Range Energy Transport. In the weak coupling limit, the polymer chains can be viewed as a series of chromophores that retain their individual geometric and electronic structures (this approximation has been carefully examined and found in the present case to be a reasonable assumption, vide infra; this eliminates the need to perform time-consuming supermolecular calculations). The ground-state [excited-state] geometries of methyl-substituted indenofluorene oligomers (used here to model the tetraethylhexyl indenofluorene units of the actual system) and of the perylene derivatives were optimized at the AM1 [AM1/CAS-CI][38] level assuming planar conformations. To model *intermolecular* energy transfer, donor/acceptor complexes consisting of cofacial dimers with parallel longitudinal axes and superimposed centers have been built. The geometric structure of these complexes was optimized at the Molecular Mechanics level with the Dreiding force field;[39] we considered various starting relative orientations while freezing the *intramolecular* structural parameters to their AM1-optimized values; we also explored the influence of longitudinal and rotational motions on the excitation dynamics. These optimized geometries were then used as input for excited-state calculations performed at the INDO/SCI level.[40] As output of these calculations, we obtain the excitation energies and transition dipole matrix elements. As described above, the electronic couplings are calculated in the framework of the distributed monopole model (DMM), on the basis of the atomic contributions to the INDO/SCI transition dipole moments.

To model long-range exciton migration along the polymer chains, the time-dependent occupation probability on site m, $P_m(t)$, is obtained by solving the following set of Pauli master equations[20] (PME):

$$\frac{\partial}{\partial t}P_m(t) = -\sum_{n\neq m}(k_{mn}P_m(t) - k_{nm}P_n(t) + P_m\tau_m^{-1}) \quad (14)$$

where k_{mn} is the rate for excitation energy transfer from site m to site n as given by eq 1 and τ_m is the (radiative) lifetime for the excitation on the site m. The first term on the right-hand side of eq 14 describes the decay with time of $P_m(t)$ as a result of exciton migration from site m to all other sites; the second term is associated with the reverse hopping to site m from all sites $n \neq m$; the last term accounts for the natural exciton lifetime in the absence of any transfer process. Radiative lifetimes associated to each site m,τ_m, have been calculated from the corresponding Einstein coefficient for spontaneous emission:

$$\tau_m^{-1} = \left(\frac{8\pi^2\nu_{fi}^3}{3\epsilon_0\hbar c^3}\right)|\mu_{fi}|^2 \quad (15)$$

where ν_{fi} and μ_{fi} are the INDO/SCI absorption frequency and transition dipole moment calculated for the *relaxed* $f\rightarrow i$ electronic excitation on site m.

From the solution of these equations (obtained through numerical diagonalization of the stochastic matrix defined by the transfer rates),[41] one can derive a series of useful observables, which allows for a direct comparison to the experimental data. In particular, the time-dependent population on the perylene moiety can be compared directly to the measured time-resolved perylene photoluminescence spectrum. In addition, the mean value of any observable o, such as electronic excitation energy, emission anisotropy, or migration distance, can be readily obtained at any time t:

$$\langle o\rangle(t) = \sum_{\mathrm{m}} P_m(t)\, o(m) \quad (16)$$

Time-dependent photoluminescence spectra of the whole system can be computed for instance from the time-dependent occupation probabilities ($P_m(t)$) and emission spectra associated to each site ($o(m)$ in eq 16). To provide a relevant description of the system under investigation, a large number of chains (typically 1000 chains) were generated by means of Monte Carlo simulations from various distributions of chromophore conjugation lengths. Ensemble properties were obtained by averaging over all the generated configurations. The procedure was repeated for chain sizes that are consistent with the experimental polymer length distributions.

III. Experimental Results

The synthesis of this class of materials has been described previously.[42] Polymer samples were dissolved in anhydrous *p*-xylene in a nitrogen environment to avoid contact of either polymer or solvent with air. Films of ~150 nm thickness were prepared in a nitrogen glovebox by spin-coating the polymer solution onto Spectrosil substrates. Samples were stored under nitrogen prior to use, and films were kept under dynamic vacuum ($<10^{-5}$ mbar) during experiments to prevent photooxidation. The time-correlated single-photon counting and photoluminescence up-conversion measurements were performed as described previously.[43,44]

Time-Resolved Spectroscopy Measurements in Solutions and Films. The spectral overlap of the PIF photoluminescence (PL) spectrum with the perylenemonoimide (PI) absorption spectrum ensures RET from PIF to PI.[43] Excitation in the blue region of the spectrum (~3.1 eV for all the spectra given herein) accesses the $\pi-\pi^*$ transition in the PIF backbone (see absorption spectrum in Figure 2a), with essentially no direct excitation of the PI units. The latter have their absorption maximum in the green region (2.33 eV). The time-integrated PL spectrum of a PEC-PIFTEH solution (1.7 g/L in *p*-xylene) is displayed as a continuous line in Figure 2b. Approximately equal contributions of emission from the polymer chain (2.3−3.0 eV) and dye endcaps (1.8−2.3 eV) are observed, indicating that exciton transfer from the polymer to the dye occurs in competition with the excited-state decay of the polymer. Figure 2 also shows the absorption (a) and time-integrated PL spectrum (b) of a PEC-PIFTEH film (broken line), which is dominated by PI emission. The differences in the time-integrated PL spectra between solutions and films arise from a roughly 2 orders of magnitude difference in the energy-transfer time scale in the two environments; this is shown in Figures 2 (c and d) and 3. Time-resolved PL spectra are displayed in Figure 2 both for a 0.15-g/L

(38) Dewar, M. J. S.; Zoebisch, E. G.; Healy, E. F.; Stewart, J. J. P. *J. Am. Chem. Soc*. **1995**, *107*, 3702.
(39) Mayo, S. L.; Olafson, B. D.; Goddard, W. A., III. *J. Phys. Chem.* **1990**, *94*, 8897.
(40) Ridley, J.; Zerner, M. C. *Theor. Chim. Acta* **1973**, *32*, 111.
(41) Bacchiocchi, C.; Zannoni, C. *Chem. Phys. Lett.* **1997**, *268*, 541.
(42) Ego, C.; Marsitzky, D.; Becker, S.; Zhang, J. Y.; Grimsdale, A. C.; Mullen, K.; MacKenzie, J. D.; Silva, C.; Friend, R. H. *J. Am. Chem. Soc*. **2003**, *125*, 437.
(43) Herz, L. M.; Silva, C.; Friend, R. H.; Phillips, R. T.; Setayesh S.; Becker, S.; Marsitsky, D.; Müllen, K. *Phys. Rev. B* **2001**, *64*, 195203.

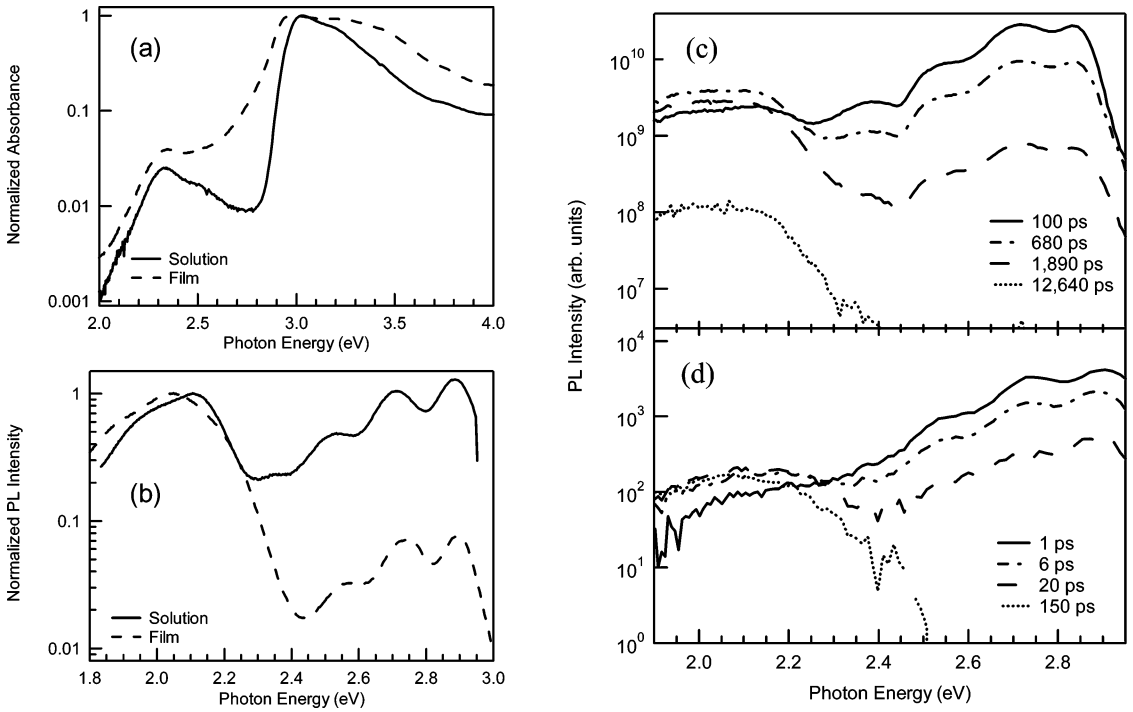

Figure 2. Experimental absorption (a) and photoluminescence (b) spectra of PEC-PIFTEH in 1.7 g/L solution in *p*-xylene (continuous line) and in a thin film (broken line). Time-resolved photoluminescence spectra of PEC-PIFTEH in a 0.15 g/L solution in *p*-xylene (c) and in a thin film (d). The delays after pulsed excitation are given in the inset of each panel. The spectra in parts (c) and (d) were measured using time-correlated single photon counting and photoluminescence up-conversion techniques, respectively.

solution in *p*-xylene (c) and a thin film (d). In both environments, the PL spectrum at early time after excitation with a laser pulse is dominated by that of the PIF backbone.[45] This early-time PIF signature evolves into a feature centered in the yellow-red part of the spectrum, characteristic of PI emission. The time scale in which this evolution occurs is dramatically shorter in the film. This is further demonstrated in Figure 3, which plots the PL decay in the blue (filled circles) and green (open squares) regions in solution and film. The (1/e) − decay time of the PL arising from the PIF backbone is approximately 500 ps. This also corresponds to the time constant of emergence of PL arising from the PI acceptor. In contrast, these (1/e) − decay times diminish to approximately 5 ps in the film.

The enhanced rate of energy transfer in the film is a result of the large number of intermolecular contacts between donor and acceptors leading to the emergence of additional pathways for the excitation energy and the favorable interchain electronic coupling distribution between PIF and PI chromophores, vide infra. Note that exciton diffusion within the host is expected to play a significant role only if the effective guest concentration is low as a result of phase segregation effects. In a PEC-PIFTEH film, where PI units are coupled covalently to the polymer backbone such that there is a high number of PIF/PI intermolecular interactions, there is a high yield of direct resonance energy transfer without the need for excitons to diffuse near an acceptor. Even with a relatively low acceptor density, nearly complete energy transfer is achieved.

Physical Length Distributions. To determine the chain-length distribution in the polymer sample, gel permeation chromatography (GPC) measurements have been performed using polystyrene as a standard for the calibration. As is usually found for rigid-rod polymers, this procedure leads to a systematic overestimation of the molecular weights. Assuming a 60% contraction factor to correct for this error, the resulting number average and weight average molecular weights are estimated to be 11000 and 40000, respectively, corresponding to an average chain length of about 14 indenofluorene units.

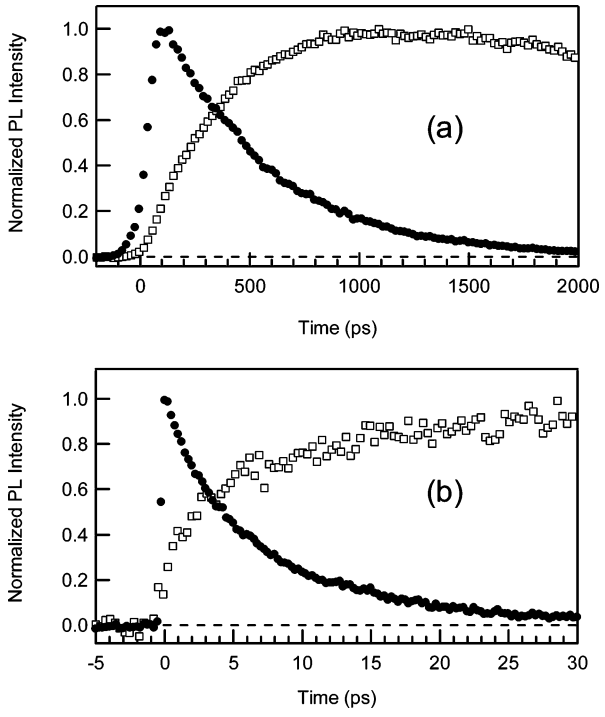

Figure 3. (a) Time-resolved photoluminescence intensity at 2.740 eV (solid circles) and 2.000 eV (open squares) in a 0.05 g/L solution in *p*-xylene. The solution was excited at 3.046 eV photon energy. The data were measured using time-correlated single photon counting. (b) Same as part (a), but in a thin film excited with 3.1 eV photon energy. The data were measured using photoluminescence up-conversion techniques.

(44) Morteani, A. C.; Dhoot, A. S.; Kim, J. S.; Silva, C.; Greenham, N. C.; Murphy, C.; Moons, E.; Cina, S.; Burroughes, J. H.; Friend, R. H. *Adv. Mater.* **2003**, *15*, 1708; Hayes, G. R.; Samuel, I. D. W.; Philips, R. T. *Phys. Rev. B* **1995**, *52*, 11569.

(45) Silva, C.; Russell, D. M.; Stevens, M. A.; MacKenzie, J. D.; Setayesh, S.; Müllen, K.; Friend, R. H. *Chem. Phys. Lett.* **2000**, *319*, 494; Beljonne, D.; Pourtois, G.; Silva, C.; Hennebicq, E.; Herz, L. M.; Friend, R. H.; Scholes, G. D.; Setayesh, S.; Müllen, K.; Brédas, J.-L. *Proc. Natl. Acad. Sci. U.S.A.* **2002**, *99*, 10982.

We stress that there is a very large uncertainty on this number because, in addition to the intrinsic error on molecular weight determination from GPC measurements of rigid polymer chains and the large polydispersity (≫3.6) of the sample, single molecular spectroscopy experiments indicate that a large fraction of the polymer chains (∼60%) actually bear a single perylene dye at one extremity, the remaining 40% being endcapped at both ends.[46] Another estimate for the mean physical chain length can be obtained from the relative contributions of the polymer chain and the perylene group to the absorption spectrum. A ratio on the order of 47 is obtained for the PIFTEH over PEC contributions to the optical absorption by integrating the solution spectrum between 1.77 and 2.76 eV (PEC absorption) and between 2.76 and 4.2 eV (PIFTEH absorption). On the basis of the oscillator strength calculated for one perylene derivative (0.93 from INDO/SCI calculations) and for individual repeat units in the polyindenofluorene chains (an average value of 1.3 per unit has been determined from oscillator strengths computed at the INDO/SCI level for OIF_n oligomers of varying size), an average polymer length on the order of 34 and 68 indenofluorene units has been determined when assuming polymer chains endcapped at one extremity and at both ends, respectively. Because of the large fraction of chains that are mono endcapped and the uncertainty on the distribution of total chain lengths, the simulations of long-distance exciton transport have been performed for polymer chains of increasing size (ranging from 10 to 100 repeat units) carrying only one perylene dye.

IV. Electronic Structure and Optical Properties of Oligoindenofluorenes

As pointed out previously, conjugated polymers are usually characterized by inhomogeneously broadened absorption spectra as well as excitation-energy dependent energy-transfer dynamics. These two features are accounted for in models where the polymer chains are pictured as an ensemble of chromophores (separated by chemical or structural defects) with a statistical distribution of conjugation lengths. The photophysical properties of disordered polymeric materials are thus strongly reminiscent of the corresponding spectral characteristics in the oligomers. Therefore, we have explored the electronic structure and optical properties of indenofluorene oligomers with increasing size (ranging from 2 to 8 units) as these are directly relevant to understanding the excitation motion dynamics in the polymer.

Excitation Energies and Geometric Relaxation Phenomena. The INDO/SCI vertical transition energies computed on the basis of the AM1 ground-state geometries decrease linearly with the inverse number of repeat units, as expected from increased conjugation lengths (see Figure 4a). When considering oligomers in their relaxed excited-state geometries, a linear relationship between the electronic excitation energies and the inverse chain length is obtained for oligomer sizes ranging from 1 to 3 units; the transition energy is only weakly modified by further increasing the chain length and converges to ∼2.98 eV in the long chain limit (which only differs from the excitation energy of the trimer by 0.02 eV). The very similar excitation energies calculated for the tetramer, hexamer, and octamer of indenofluorene can be attributed to the similar amounts of delocalization in the corresponding wave functions (see below). Note that the calculated 0−0 excitation energies compare favorably to the experimental values, which evolve from 3.2 eV in the dimer to 3.0 eV in the hexamer (compared to 3.28 and 3.08 eV, respectively, at the INDO/SCI level).

(46) Jäckel, F.; De Feyter, S.; Hofkens, J.; Köhn, F.; Rousseau, E.; De Schryver, F. C.; Ego, C.; Müllen, K. Unpublished results.

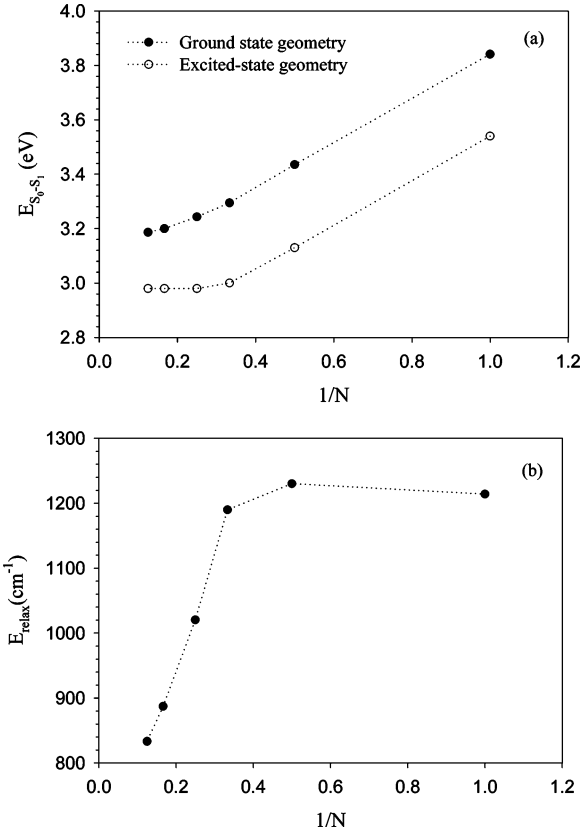

Figure 4. (a) Evolution with inverse chain length of the INDO/SCI excitation energies, as computed on the basis of the ground- and excited-state geometries of oligo(indenofluorene)s. (b) Evolution with inverse chain length of the relaxation energy associated with geometric deformations taking place on going from the ground to the excited electronic state in oligo(indenofluorene)s when planar conformations are assumed. *N* is the number of repeat units.

Upon geometric relaxation in the excited state, changes in bond lengths occur toward a more quinoidic structure, with a shortening of the inter-ring C−C bonds and a more planar structure. Strong geometric deformations take place around the central part of the molecule and then decrease on moving away from the center to the edges. The confinement of the geometric distortions in the middle of the conjugated chains leads to a self-localization of the excited-state wavefuntion in this area (around a few repeat units, vide infra).

The decrease in excitation energy with inverse chain length is more pronounced when considering ground-state geometries, indicating a decrease in the displacement in equilibrium geometry on going from the ground state to the lowest singlet excited state. As a matter of fact, the relaxation energy (defined as the difference between vertical and adiabatic electronic transitions) shows a marked decrease with increasing chain length for oligomer sizes larger than ∼2−3 repeat units (which corresponds to the "natural" size of the structural relaxation induced by photoexcitation),[30,47] see Figure 4b. It is important to stress that in all cases, the computed relaxation energies are typically 1 order of magnitude larger than the electronic couplings, which supports the use of an incoherent hopping model among localized chromophores to depict the energy migration dynamics.

Degree of Delocalization in the First Excited State. The degree of delocalization in the first excited state can be evaluated

(47) Shuai, Z.; Brédas, J. L.; Su, W. P. *Chem. Phys. Lett.* **1994**, *228*, 301.

Table 1. Participation Ratios, PR, Computed for Indenofluorene Oligomers OIF_n, in Their Ground- and Excited-State Geometries

oligomer size	PR (ground-state geometry)	PR (excited-state geometry)
1	1.0	1.0
2	2.0	2.0
3	2.4	2.1
4	3.0	2.4
6	4.0	2.6
8	5.9	2.7

using the so-called participation ratio, PR,[48] defined as:

$$\mathrm{PR} = \frac{\sum_{i=1}^{N} C_i^2}{\sum_{i}^{N} C_i^4} \tag{17}$$

where C_i^2 represents the contribution of site labeled *"i"* to the excited-state wave function. PR can be regarded as the number of sites coherently coupled in the excited state. The participation ratio ranges from N (the total number of sites in the system) for a completely delocalized wave funtion (in this case, $C_i = 1/\sqrt{N}$, for any i) to 1 for localization on a single site.

As a result of strong electronic interactions between neighboring indenofluorene units within a conjugated chromophore, the wave function associated with the first electronic excited state can be partitioned into a superposition of electronic excitations localized on each site i, $|\varphi_i\rangle$, and charge-transfer transitions, $|\varphi_{ih,je}\rangle$, arising from excitation of one electron from site i to all other sites j:

$$\psi = \sum_i c_i |\varphi_i\rangle + \sum_i \sum_j c_{i\rightarrow j} |\varphi_{ih,je}\rangle \tag{18}$$

The contribution from each site i to the overall excited-state wave function is then calculated according to:

$$C_i^2 = c_i^2 + \frac{1}{2}\sum_j c_{i\rightarrow j}^2 \tag{19}$$

Two-particle electron−hole wave functions[49] can be readily obtained from the SCI calculations and decomposed into localized (c_i) versus charge-transfer ($c_{i\rightarrow j}$) contributions. These can then be injected into eqs 19 and 17 to calculate the participation ratios. The PRs obtained in the first singlet excited states of oligo(indenofluorene)s are given in Table 1 for both ground- and excited-state geometries.

In the monomer and dimer cases, the excited-state wave functions spread over the whole structure, whatever the chosen geometry. As the number of repeat units increases, the wavefuntion no longer extends over the whole molecule; it gets confined around the center with decreasing amplitude toward the ends (the PR value becomes smaller than the number of repeat units). This effect is much more pronounced in the excited-state geometry where, as a result of the self-confinement induced by lattice relaxation, the excited-state wave function shows dominant contributions over a section of the chain that does not exceed an indenofluorene trimer in size (PR ranges from 2 to 2.7 units when considering a chromophore length ranging from 3 to 8 repeat units).

Insight into the extent of localization/delocalization in the first singlet excited state can also be gained by considering the spatial distribution of the transition densities induced by photoexcitation into this state. Such distributions are displayed in Figure 5 for the tetramer, hexamer, and octamer of indenofluorene in their relaxed and unrelaxed geometries. The increase in the amount of delocalization with oligomer length is much more pronounced in the ground-state geometry while the wave function computed in the excited-state geometry is found to remain confined to the central dimer with slight contributions from the covalently attached neighboring sites. Such an evolution is fully consistent with the analysis based on the participation ratios.

Optical Spectra and Radiative Lifetimes. From time-dependent perturbation theory, the integrated absorption coefficient associated with an electronic transition from the ground

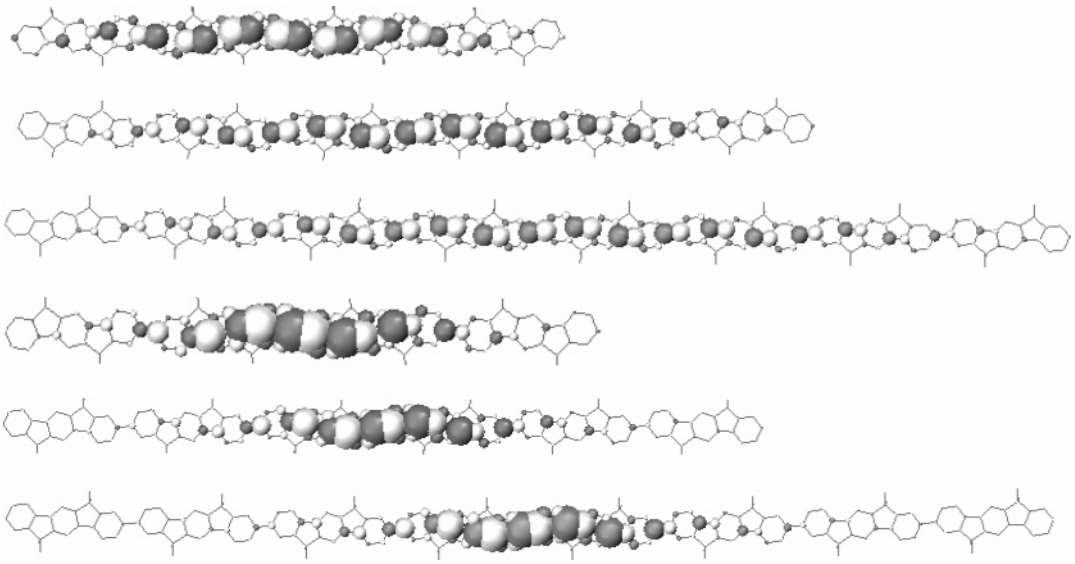

Figure 5. Spatial distribution of the atomic transition densities associated with the first singlet excited state as computed at the INDO/SCI level. From top to bottom: transition densities computed for OIF_4, OIF_6, and OIF_8 in their ground-state geometries and the same sequence for the excited-state geometries.

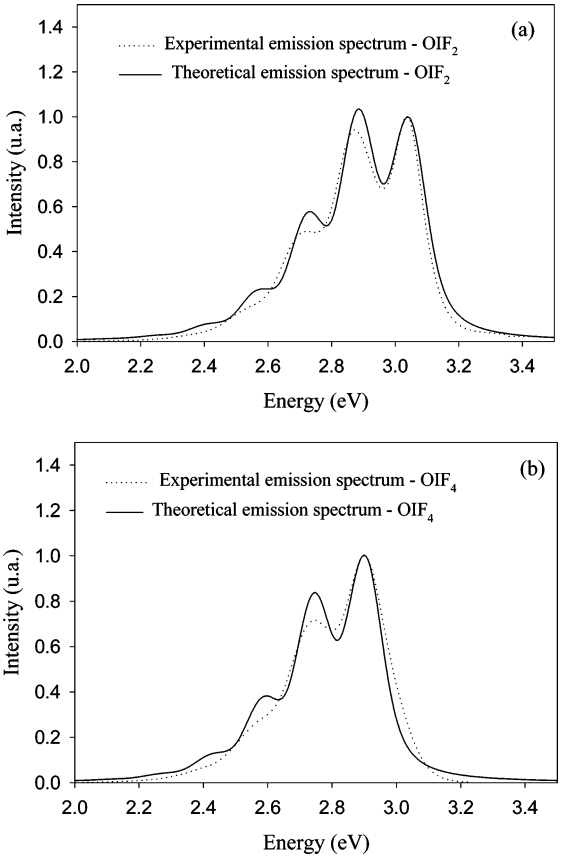

Figure 6. Experimental (dotted line) and theoretical (full line) emission spectra of the indenofluorene dimer OIF_2 (a) and tetramer OIF_4 (b). The theoretical spectra have been red-shifted (by 0.08 eV in both OIF_2 and OIF_4) to have the calculated and measured 0−0 lines superimposed.

state to an excited state is proportional to the product of the corresponding transition dipole moment squared and the transition energy; the peak intensity in emission scales with the squared transition dipole moment and the third power of the corresponding transition energy. As a result of increasing transition dipole moment with increasing oligomer size, the intensity of the absorption and emission peaks raises with oligomer length, yet this effect is less pronounced in emission as a result of the excited-state localization driven by vibrational relaxation (all spectra are provided in Supporting Information). The absorption and emission spectra computed for the perylene derivative show significantly less intense features compared to oligo(indenofluorene)s, as a result of the smaller transition dipole moment: the ratio between the oligo(indenofluorene)s and perylene transition moments increases from 1 to 3 with increasing oligomer length.

As an illustration, the experimental and theoretical emission spectra obtained for the indenofluorene dimer and tetramer are displayed in Figure 6. Despite the simplicity of the model, the calculations reproduce very well the measured vibronic progression. In particular, the increased relative intensity of the electronic 0−0 line in the longer segment is well described; it is indicative of less pronounced geometric deformations and

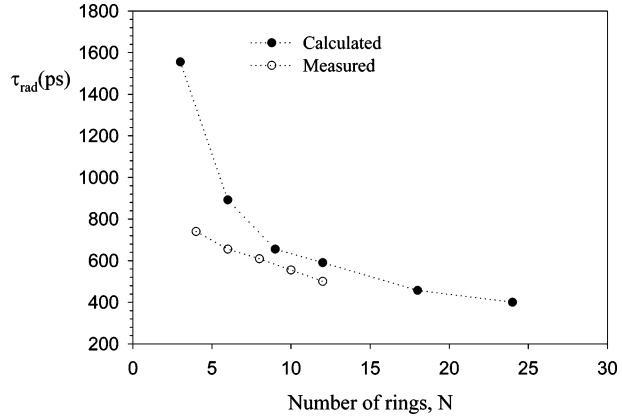

Figure 7. Calculated radiative lifetimes in indenofluorene oligomers and corresponding measured values for fluorene oligomers of varying size. *N* denotes the number of phenylene rings.

smaller relaxation energy. Photoluminescence spectra calculated and measured for longer oligomers (not shown) do not show appreciable changes with respect to the tetramer case.

The radiative lifetimes computed at the INDO/SCI level for indenofluorene oligomers are compared to experimental values obtained for solutions of oligofluorenes in Figure 7. The lifetimes are plotted as a function of the number of phenylene rings to allow for comparison between oligo(fluorene)s and oligo(indenofluorene)s of similar sizes (to the best of our knowledge, radiative lifetimes have not been reported for indenofluorene oligomers). The computed radiative lifetimes for the tetramer, hexamer, and octamer of indenofluorene, which are the main building blocks of our system, range from 600 to 400 ps; these values are consistent with the experimental data reported for oligomers of fluorene[50] of similar lengths (Figure 7). For instance, the experimental radiative lifetime obtained for the fluorene hexamer amounts to about 500 ps, in close agreement with the 590 ps lifetime calculated for the indenofluorene tetramer.

Chromophores and Conjugation Length Distributions. The quantum-chemical calculations indicate that, in the *relaxed excited-state geometry*, the electronic excitations do not extend over more than 3 repeat units. Such an effective size for the "donor" wave functions is consistent with the leveling off of the measured photoluminescence properties in oligo(indenofluorene)s containing more than ∼3−4 units as discussed above. The effective size for the "acceptor" wave functions is more difficult to assess as it is very sensitive to the degree of conformational motion, which is likely to be different in solutions and in films. According to the spectroscopic investigation by Setayesh et al.,[51] an average conjugation length of ∼6−7 units is inferred from comparison of indenofluorene oligomer and polymer absorption spectra; this is close to the value of the participation ratio calculated for a long polymer segment (PR ∼6 in OIF_8).

In addition, the polymer absorption spectrum, shown in Figure 2a, closely resembles the corresponding spectra of long oligomers (see supplementary information), pointing to a rather narrow distribution of conjugation lengths in the range 4−6 units. Hence, in the simulations of long-range transport, we

(48) Fidder, H.; Knoester, J.; Wiersma, D. A. *J. Chem. Phys.* **1991**, *95*, 7880; Schreiber, M.; Toyozawa, Y. *J. Phys. Soc. Jpn.* **1982**, *51*, 1528.
(49) ZOA V2.0, J. P. Calbert, Labratory for Chemistry of Novel Materials, Mons Belgium; see also, e.g.: Zojer, E.; Buchacher, P.; Wudl, F.; Cornil, J.; Calbert, J. Ph.; Brédas, J. L.; Leising, G.; *J. Chem. Phys*. **2000**, *113*, 10002; Rissler, J.; Bässler, H.; Gebhard, F.; Schwerdtfeger, P. *Phys. Rev. B* **2001**, *64*, 045122.
(50) Lupton, J. M.; Craig, M. R.; Meijer, E. W. *Appl. Phys. Lett.* **2002**, *80*, 4489.
(51) Setayesh, S.; Marsitzky, D.; Müllen, K. *Macromolecules* **2000**, *33*, 2016.

Table 2. Spectral Overlap Factors Computed for OIF_n to OIF_m and OIF_n to PEC Energy Transfer, as Calculated on the Basis of a Two-Mode Model and (between parentheses) a Single-Mode Model, See Text

		spectral overlap factors J_{DA} (eV^{-1})					
A	D	OIF_1	OIF_2	OIF_3	OIF_4	OIF_6	OIF_8
OIF_1		0.178 (0.83)	0.023 (0.11)	0.019 (0.08)	0.0169 (0.07)	0.017 (0.07)	0.016 (0.07)
OIF_2		1.37 (1.05)	0.106 (0.76)	0.070 (0.38)	0.0589 (0.38)	0.057 (0.36)	0.056 (0.34)
OIF_3		1.52 (0.77)	0.276 (1.14)	0.146 (0.8)	0.116 (0.8)	0.11 (0.77)	0.107 (0.75)
OIF_4		1.16 (0.65)	0.43 (1.26)	0.2 (1.0)	0.15 (1.0)	0.14 (0.98)	0.138 (0.97)
OIF_6		1.016 (0.56)	0.56 (1.32)	0.247 (1.12)	0.18 (1.12)	0.17 (1.13)	0.164 (1.13)
OIF_8		0.96 (0.53)	0.63 (1.33)	0.275 (1.17)	0.198 (1.17)	0.18 (1.19)	0.18 (1.19)
PEC		0.08 (0.13)	0.94 (0.6)	1.1 (0.87)	1.26 0.87)	1.34 (0.88)	1.377 (0.88)

considered as a representative model for the actual polymer a distribution peaking at the hexamer and with a width of two repeat units (i.e., 50% of hexamers, 25% of tetramers, and 25% of octamers). Although there is some uncertainty on the distribution width, its precise choice does not strongly impact the excitation diffusion dynamics (as fluctuations in the excitation and relaxation energies are only minor for segments larger than four units).

V. Modeling Intrachain and Interchain Excitation Migration Processes

To provide a quantitative description of *intrachain* versus *interchain* energy transfer in PEC-PIFTEH and therefore to rationalize the different dynamics observed in solution and in film, we first modeled the elementary excitation transfer processes taking place among conjugated segments of the PIF polymer chains as well as from these segments to the perylene endcaps; in both cases, nearest-neighbor intrachain and interchain energy migration phenomena are considered. In a second step, long-range intramolecular exciton transport along polyindenofluorene strands capped at one end with a perylene derivative is explored. The overall excitation energy funneling along the polymer backbone and the trapping dynamics are modeled in the absence of any chain-to-chain contact, thus considering a fully extended (rigid-rod) PIF chain.

Single Hopping Steps. Electronic couplings, spectral overlaps and energy-transfer rates have been computed for a number of covalently linked donor/acceptor segments, considering indenofluorene oligomers ranging in size from 1 to 8 repeat units. Both nondirectional (involving chromophores of the same length and therefore characterized by identical excitation energies) and directional (transfer from higher to lower energy sites) energy-transfer processes have been assessed. Note that for nondirectional excitation migration, backward and forward transfers occur at the same rate, resulting in a random walk of the excitation energy before trapping on a lower energy site (either a more extended oligoindenofluorene segment or a perylene endcap). Homomolecular (to be understood here as taking place among chromophores of the same chemical nature, i.e., indenofluorene oligomers) and heteromolecular (taking place between chromophores of different chemical natures, i.e., from the oligoindenofluorene segments to the perylene endcaps) energy-transfer processes have been investigated considering both intrachain and interchain motion. In the latter case, the simulations were performed for donor/acceptor complexes wherein the two chromophores are packed in a cofacial arrangement. For each donor/acceptor pair, molecular mechanics calculations have been carried out to determine the equilibrium *intermolecular* geometric parameters. The center-to-center donor−acceptor separation is calculated to be close to 4.2 Å when considering methyl groups as side chains in the simulations (similar results are obtained for model systems when accounting for the full chemical structure of the side chains). We will discuss successively the results of the calculations on spectral overlaps, electronic coupling factors, and transfer rates and focus on the comparison between *intrachain* and *interchain* processes.

Spectral Overlaps. As described in section II, the spectral overlaps have been computed on the basis of the optical absorption and emission spectra simulated within a displaced harmonic oscillator model and retaining two effective vibration modes (a high-frequency mode representative of the dominant changes in bond lengths and a low-frequency mode associated with the changes in conformation toward a more planar structure in the excited state).

Spectral overlap factors computed for various OIF_n/OIF_m and OIF_n/PEC pairs on the basis of the simulated and measured normalized donor emission and acceptor absorption spectra are presented in Table 2 and illustrated in Figure 8. When considering homomolecular transfer, the spectral overlap is found to increase with increasing acceptor size for a given donor size, while it decreases with increasing donor size for a given acceptor (see Table 2). These evolutions are the result of a subtle interplay between geometric relaxation energies (E_{rel}^{D}) and shifts in the optical spectra due to changes in chromophore conjugation lengths Δ^{DA}. When the former exceed the latter (as is the case here, except in the short oligomers), the spectral overlap is maximized for long acceptor chains and short donors, leading to the smallest mismatch between E_{rel}^{D} and Δ^{DA}, see scheme below:

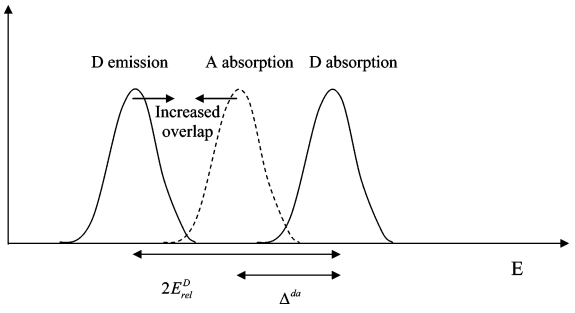

Note that the spectral overlap factors computed in the case of heteromolecular transfer are found to be larger than the homomolecular counterparts whatever the donor size. Spectral overlap factors obtained when taking into account only the high frequency mode are also reported in Table 2. These are approximatively 1 order of magnitude larger than the values

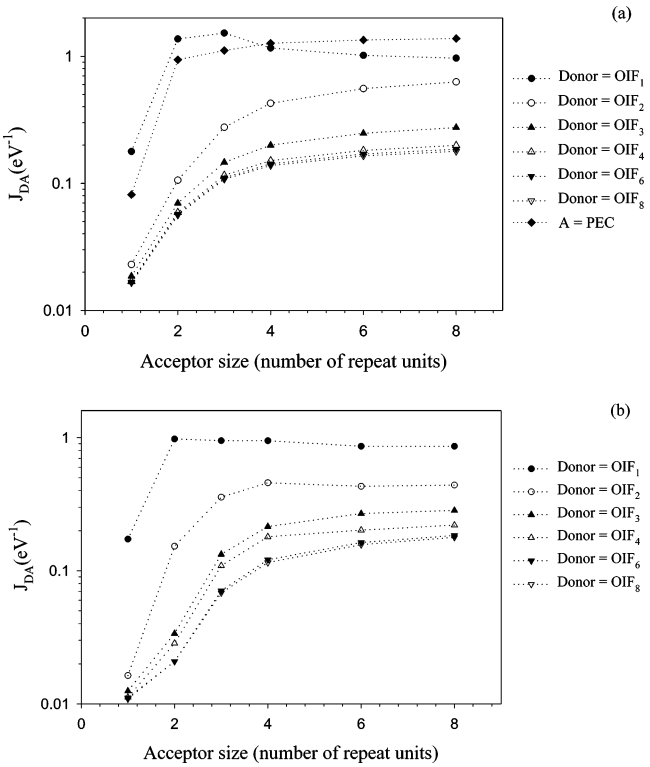

Figure 8. Spectral overlap factors computed for various OIF_n/OIF_m and OIF_n/PEC pairs on the basis of the simulated (a) and measured (b) normalized donor emission and acceptor absorption spectra. Oligomers of indenofluorene with a conjugation length ranging from 1 to 8 units have been considered.

obtained when the effective libration mode is included. Such differences result from the significant Stokes shift ($\gg$0.2−0.3 eV) associated to coupling of soft modes to the electronic transitions and the concomitant red shift in emission and blue shift in absorption. Thus, when electronic transitions are coupled to low frequency modes, as libration modes in floppy polymer chains, the spectral overlap integrals get strongly reduced resulting into slower energy migration.[14,52] It follows that fully ladder-type structures, where all phenylene units are forced to lie in the same plane, should lead to improved transport along the polymer chains.

Electronic Couplings. Electronic coupling matrix elements V_{DA} have been computed for both heteromolecular and homomolecular on-chain and *interchain* energy transfer using the distributed monopole model on the basis of relaxed excited-state geometries. The results are given in Table 3 (see also the Figures in supplementary information) for *intrachain* and *interchain* processes. The electronic couplings for on-chain exciton hopping are computed for several covalently linked OIF_n/OIF_m and OIF_n/PEC donor−acceptor couples, while the electronic matrix elements for interchain energy transfer are given for several OIF_n/OIF_m and OIF_n/PEC complexes differing by the size *n*, *m* of the oligomers.

When considering *intrachain* processes, electronic couplings computed for both homomolecular and heteromolecular processes are found to drop quickly with the size of the donor and the acceptor. This arises from the increased inter-site separations, together with a decrease in the transition density at the edges

(52) Brunner, K.; Tortschanoff, A.; Warmuth, C.; Bässler, H.; Kauffmann, K. F. *J. Phys. Chem. B* **2000**, *104*, 3781.

Table 3. Intrachain and Interchain Electronic Couplings (in absolute values), as Computed on the Basis of the Distributed Monopole Model, for Several OIF_n/OIF_m and OIF_n/PEC Couples[a]

A	D	OIF_1	OIF_2	OIF_3	OIF_4	OIF_6	OIF_8
Intrachain Electronic Couplings V_{DA} (cm^{-1})							
OIF_1		965	535	313	184	86	44.5
OIF_2		702	424	262	161	79	43
OIF_3		470	297	189.7	121	62	34.8
OIF_4		346	225	147	96	51	29.3
OIF_6		222	149	100	67	37	22.1
OIF_8		162	111	75	51.5	29	17.9
PEC		1166	665	395	231	107	55
Interchain Electronic Couplings V_{DA} (cm^{-1})							
OIF_1		1008	695	483	459	428	406
OIF_2		708	888	681	647	587	555
OIF_3		433	603	604	545	480	456
OIF_4		247	409	435	447	395	370
OIF_6		109	192	221	248	261	244.5
OIF_8		67.2	124	130	144	157.4	164
PEC		1168	823	573	549	506	493

[a] The donor and acceptor size are given along the first row and the first column, respectively.

of the conformational subunits. In addition, the geometry relaxation taking place in the excited state of the donor leads to a localization of the wave function and therefore a strong decrease in the atomic transition densities located at the edges of the donor molecule (see Supporting Information). For *interchain* processes, electronic matrix elements are maximized for an acceptor size of two indenofluorene units. In all cases, the V_{DA} values obtained for *intermolecular* transfer processes are found to be larger than their *intrachain* counterparts, see Table 3. For instance, the electronic couplings for intrachain homomolecular transfer processes when the donor is a tetramer are found to decrease from 184 to 51 cm^{-1} when increasing the acceptor size, while the corresponding intermolecular processes are found to be more than twice as large and decrease from 459 to 144 cm^{-1}. Similar results are obtained when the donor is an octamer, with *intrachain* and *interchain* electronic couplings ranging from 44 to 18 cm^{-1} and from 406 to 164 cm^{-1}, respectively. For heteromolecular processes, intrachain electronic couplings decrease from 1200 down to 55 cm^{-1} for an increasing donor size, while the interchain couplings are much larger than the typical values obtained for homomolecular processes and saturate around 500 cm^{-1}.

The electronic couplings computed on the basis of DMM for interchain energy transfer systematically reach a maximum value for an acceptor size of two repeat units, see Table 3 (note that the point dipole model would predict a steady increase of V_{DA} with acceptor size). The behavior predicted at the DMM level can be rationalized in the following way. In the initial state, the excitation is trapped as a result of lattice relaxation around the central part of the donor chromophore (mostly over two to three repeat units); in contrast, the acceptor excited-state wave function is delocalized over the whole π-system since based on the ground-state geometry. When increasing the acceptor size well beyond 2 units, the acceptor excited state extends over a larger area than the donor excited state, resulting in reduced electronic coupling matrix elements. Intuitively, we can expect a peak in Coulombic interactions for similar extents of the excitation delocalization on the donor and the acceptor. To check this hypothesis, DMM electronic matrix elements have been computed while neglecting geometric relaxation prior to energy transfer. In this case, the donor and acceptor excitations both

spread over the whole π-conjugated pathway; maximized V_{DA} values are then indeed obtained for donor and acceptor chromophores of comparable lengths.

The size-dependent interchain V_{DA} values can also be rationalized qualitatively by expanding the total dipole moments into contributions associated to each repeat unit.[53] The overall coupling can then be recast as a sum over electrostatic interactions between a set of partial point dipoles distributed over the donor and acceptor molecules, with each interaction term decreasing with the inverse cubic power of the dipole−dipole interdistance and depending on their relative orientations, see scheme below:

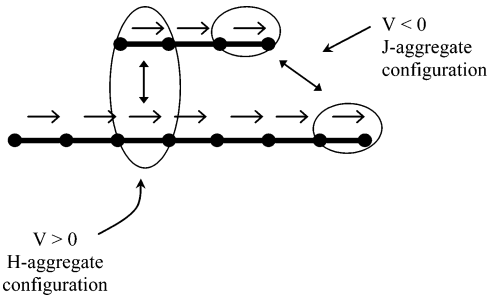

For interacting chains of the same size lying in a cofacial arrangement, positive contributions (*H*-aggregate-like) terms arise from point dipoles facing each other along the donor and acceptor chains while negative contributions (*J*-aggregate-like) are associated to more distant interactions. In the long chain limit, the weaker but more numerous *J* negative interactions annihilate the *H* positive one, leading to a vanishingly small electronic coupling.[54] The same scenario applies to chains of different sizes, with an increasing number of such negative interaction terms with increasing differences in donor and acceptor lengths.

Influence of Donor−Acceptor Relative Orientations. Up to now, we have discussed the results of interchain energy-transfer dynamics based on the equilibrium geometries of OIF_n/OIF_m or OIF_n/PEC complexes as obtained from molecular mechanics calculations. We now explore the influence of translation and rotation motions, taking as a model system the hexamer of indenofluorene as donor and the perylene derivative as acceptor.

To explore the sensitivity of the transfer rates on the relative orientations of the donor and acceptor molecules, we have considered the effects of simultaneous longitudinal translations (along the chain axis, by 2 Å step) and rotations (along the packing axis, from 0° to 360° with a 5° step) of the perylene unit with respect to an indenofluorene hexamer, see top of Figure 9. Figure 9 also shows the contour plot diagrams of the electronic couplings V_{DA} obtained within the distributed monopole model, as calculated on the basis of ground- (a) and excited-state (b) AM1/CI optimized geometries of the OIF segment, respectively (the lateral displacement, along Y, is fixed to zero in these simulations). As expected, V_{DA} is maximized when the center of the perylene derivative lies on top of the middle part of the conjugated chain and the two molecular axes are parallel to one another. Note that the dependence of V_{DA} on translational motion is particularly pronounced when allowing geometric relaxation in the excited state as a consequence of the confinement of the excited-state wave function and hence transition densities around the center of the OIF segment.

Table 4. *Intrachain* and *Interchain* Transfer Rates Computed on the Basis of the Distributed Monopole Model for Several OIF_n/OIF_m and OIF_n/PEC Couples

A	D	OIF_1	OIF_2	OIF_3	OIF_4	OIF_6	OIF_8
Intrachain Energy Transfer Rates k_{DA} (ps^{-1})							
OIF_1		24	0.96	0.27	0.08	0.018	0.005
OIF_2		99	2.77	0.07	0.22	0.053	0.015
OIF_3		49	3.6	0.77	0.25	0.06	0.019
OIF_4		20	3.2	0.63	0.20	0.054	0.017
OIF_6		7	1.8	0.36	0.12	0.03	0.012
OIF_8		4	1.13	0.23	0.77	0.02	0.0084
PEC		16	60.6	25.3	9.8	2.26	0.62
Interchain Energy Transfer Rates k_{DA} (ps^{-1})							
OIF_1		26.5	1.6	0.63	0.52	0.447	0.4
OIF_2		100	12.2	4.74	3.6	2.9	2.53
OIF_3		41.7	14.7	7.8	5.0	3.7	3.27
OIF_4		10.4	10.4	5.5	4.4	3.25	2.76
OIF_6		1.76	3.02	1.76	1.64	1.7	1.4
OIF_8		0.64	1.4	0.68	0.6	0.67	0.7
PEC		12.3	93	53	56	50	49

The electronic couplings follow more or less a cosine function of the rotation angle between the OIF and PI longitudinal axes, as would be predicted by a simple point dipole model. However, more interestingly, V_{DA} remains surprisingly large in an orthogonal orientation of the donor and acceptor molecules, provided the center of the perylene derivative is significantly displaced longitudinally (along *X*) with respect to the center of the oligo(indenofluorene) chain. Figure 9a shows that the region of minimum electronic couplings is shifted away from 90° when the perylene is moved toward the extremities of the conjugated donor molecule. For instance, for a distance of ∼10 Å from the chain end, the value of V_{DA} gets minimized for rotation angles of ∼60° and ∼320°, i.e., significantly off from the orthogonal situation. The confinement of the excited-state wave function associated with the hexamer resulting from geometric relaxation leads to a similar picture yet with important quantitative differences. While in the case where geometric relaxation phenomena are neglected the rotation angle minimizing V_{DA} decreases from 100° to 0° (or increases from 300° to 360°) on decreasing the longitudinal displacement from ∼20 to ∼5 Å, the same trend is obtained for a much narrower displacement range (from ∼28 to ∼25 Å) when considering the relaxed donor geometry. Note also that the simulations performed on the basis of the ground-state geometries indicate the presence of two peaks in $|V_{DA}|$ on shifting the perylene off the top middle part of the hexamer. These can be correlated with a change from an *H*-like to a *J*-like configuration, which is accompanied by a change in sign of the electronic coupling.

Energy Hopping Rates. The *intermolecular* and *intramolecular* DMM energy-transfer rates computed for different oligoindenofluorene donor−acceptor pairs are presented in Table 4 (see also Supporting Information). Since the electronic couplings for both *intrachain* and *interchain* energy migration decrease with the size of the donor and the acceptor segments while the spectral overlap factors increase with acceptor size, the transfer rates for a given donor size are maximized for an intermediate acceptor length. Although similar trends are

(53) Morgado, J.; Cacialli, F.; Iqbal, R.; Moratti, S. C.; Holmes, A. B.; Yahioglu, G.; Milgrom, L. R.; Friend, R. H. *J. Mater. Chem.* **2001**, *11*, 278.
(54) Mcintire, M. J.; Manas, E. S.; Spano, F. C. *J. Chem. Phys.* **1997**, *107*, 8152; Beljonne, D.; Cornil, J.; Silbey, R.; Millié, P.; Brédas, J.-L. *J. Chem. Phys.* **2000**, *112*, 4749.

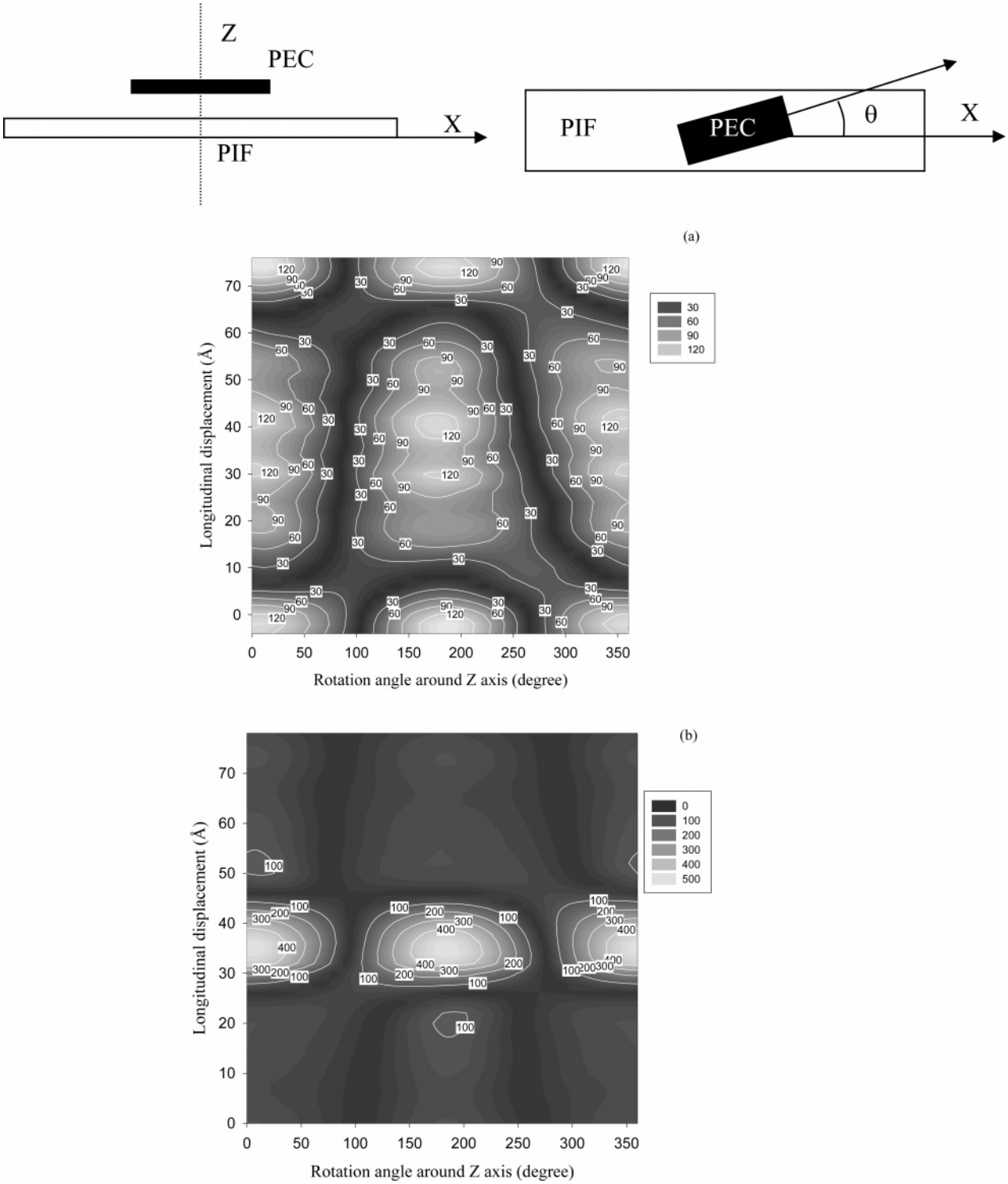

Figure 9. (Top) Schematic representation of the longitudinal (along *X*, the main molecular axis) and rotational (along *Z*, the packing axis) motions of perylene monoimide moiety with respect to the polyindenofluorene chain. (Bottom) Interchain electronic couplings, $|V_{DA}|$ (in cm^{-1}), as a function of longitudinal (along *X*) and rotational (around *Z*) motions in a OIF_6−PEC donor−acceptor pair, as calculated on the basis of the transition densities for the donor ground-state geometry (a); and on the basis of relaxed excited-state geometry (b). Note that a longitudinal displacement of 35 Å corresponds to a perfect superposition of the donor and acceptor centers.

obtained for both processes, *intermolecular* rates are always larger than the corresponding *on-chain* values for given donor and acceptor sizes.

Considering the tetramer as donor, the DMM hopping rates for intrachain processes among indenofluorene oligomers range from 0.25 to 0.08 ps^{-1}, depending on the acceptor size. The corresponding DMM intermolecular transfer rates decrease from 5 to 0.5 ps^{-1}. (Note that the use of the point-dipole model leads to much larger values, from 50000 to 250 ps^{-1}; such high rates are inconsistent with the experimental observations and would be incompatible with the weak coupling approach adopted here). For heteromolecular transfer processes, the typical intrachain rates lie in the range 60−0.6 ps^{-1}; the corresponding interchain processes are found to be up to 1 order of magnitude faster

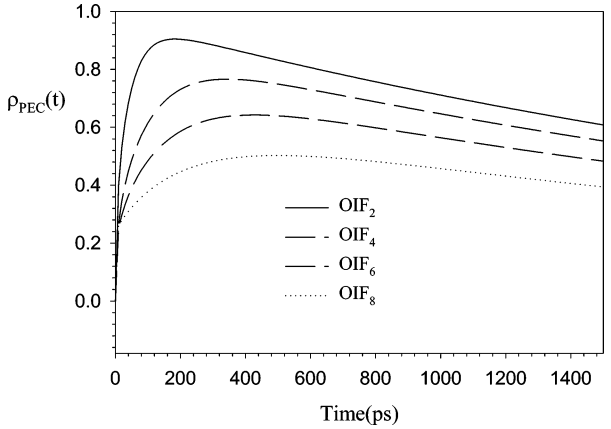

Figure 10. Time-dependent perylene population, as obtained by solving the Pauli master equations for exciton transport (eq 14) in polyindenofluorene chains endcapped with a perylene moiety. The polymer length is 30 indenofluorene units; identical building blocks of conjugation lengths 2, 4, 6, and 8 repeat units are used to generate the chains.

with rates only weakly sensitive to chain length (in the range $50-90$ ps^{-1}).

These results suggest that a much more efficient energy transfer occurs in the solid state (where chain-to-chain contacts open new efficient channels) with respect to dilute solution (assuming no direct contacts between the oligoindenofluorene segments and the perylene endcaps). This is fully consistent with the faster dynamics observed experimentally in the solid state. It is also important to point out that the calculations performed at the DMM level yield the correct order of magnitude for the interchain hopping rates, in the ps^{-1} range; a fully quantitative description is, however, difficult to achieve due to the sensitivity of the calculated electronic couplings on the relative donor−acceptor distance and separation, vide supra. In addition, while energy motion along the rigid-rod polymer chains is strictly one-dimensional, transport in the solid phase has a higher dimensionality, thereby providing a much larger interaction surface between donors and acceptors and hence many more pathways for energy transfer to the perylene emitters. A more detailed investigation of the energy migration dynamics in films taking into account both orientational and dimensionality aspects certainly warrants further work and is in progress.

Long-Range Intrachain Energy Transfer. We first investigated the influence of the chromophore conjugation length on intrachain energy migration rates by considering 30-unit long PIF polymer chains, built from identical oligofluorene segments and capped at one end by a perylene acceptor. As a result of the similar excitation energies computed for the tetramer, hexamer, and octamer of indenofluorene, the different chromophores within the system are expected to be excited with the same probability (the corresponding calculated transition energy around 3.2 eV matches the excitation energy of 3.1 eV used in the experiments). In all simulations, the excitation is thus distributed evenly among all indenofluorene oligomers at time zero. In all cases, backward transfer, nonnearest neighbor jumps, and radiative decay of the excitations are accounted for. Only backward transfer from the perylene group to the PIF segments has been neglected in our simulations (these were indeed found to be negligible compared to other OIF$_n$/OIF$_m$ and OIF$_n$/PEC donor/acceptor couples (as a result of very small spectral overlap, 8 orders of magnitude smaller than for the corresponding forward transfer). The relative efficiency for exciton migration in these different chain configurations is expected to result from a tradeoff between the number of hopping events (larger for small segments) and the mean hopping time (smaller for small segments). Figure 10 shows the time evolution of the perylene population as a function of the size of the building blocks (from 2 to 8 indenofluorene units). It turns out that, although the overall migration involves a larger number of exciton hops, the average transient time is minimized for short building blocks. This behavior arises from the fact that energy-transfer rates for the elementary processes are maximized for minimal intersite separations.

Next, we have explored the dependence of the exciton dynamics on physical chain length (L). Polyindenofluorene chains containing 12, 20, 30, 50, and 100 indenofluorene units have been built from a statistical distribution of conjugated segments close to the experimental one (50% of hexamers, 25% of tetramers, and 25% octamers for chain lengths of 20 units or larger; the 12-unit chain simply comprises 2 indenofluorene hexamers, and the 20-unit chain comprises two hexamers and one octamer). As expected, the characteristic transient time to the perylene trap, defined here as the time at which the perylene population peaks, increases, and the number of excitations that effectively reach the perylene group decreases with increasing chain length, see Figure 11a. The characteristic times for the overall migration process are on the order of 100, 300, 450 ps

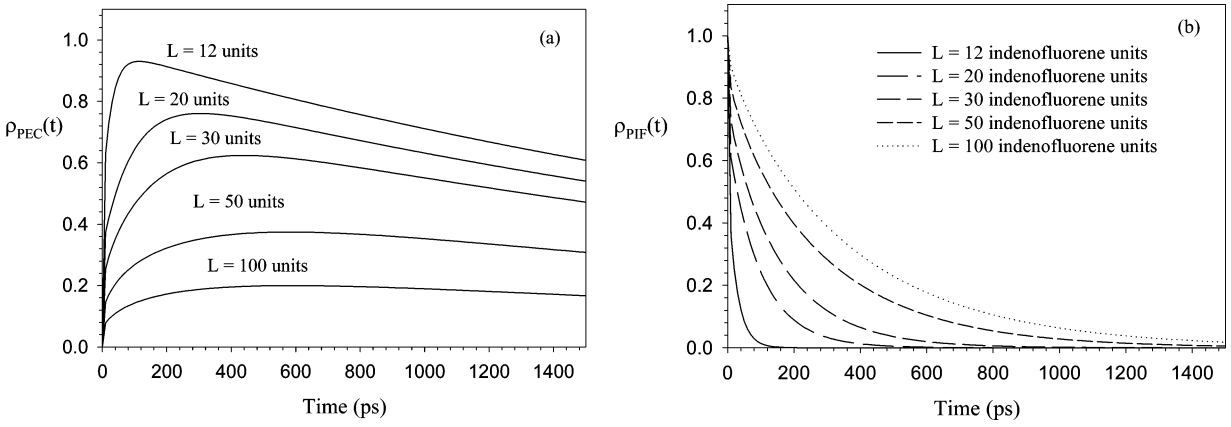

Figure 11. Time-dependent perylene population [$\rho_{PEC}(t)$] (a) and polyindenofluorene population (b) for total chain length of 12, 20, 30, 50, and 100 repeat units. A distribution of oligomer lengths close to the experimental one (50% of hexamers, 25% of tetramers and octamers) has been adopted (except for the 12-unit chain that consists of 2 indenofluorene hexamers and the 20-unit chain that consists of 2 hexamers and one octamer).

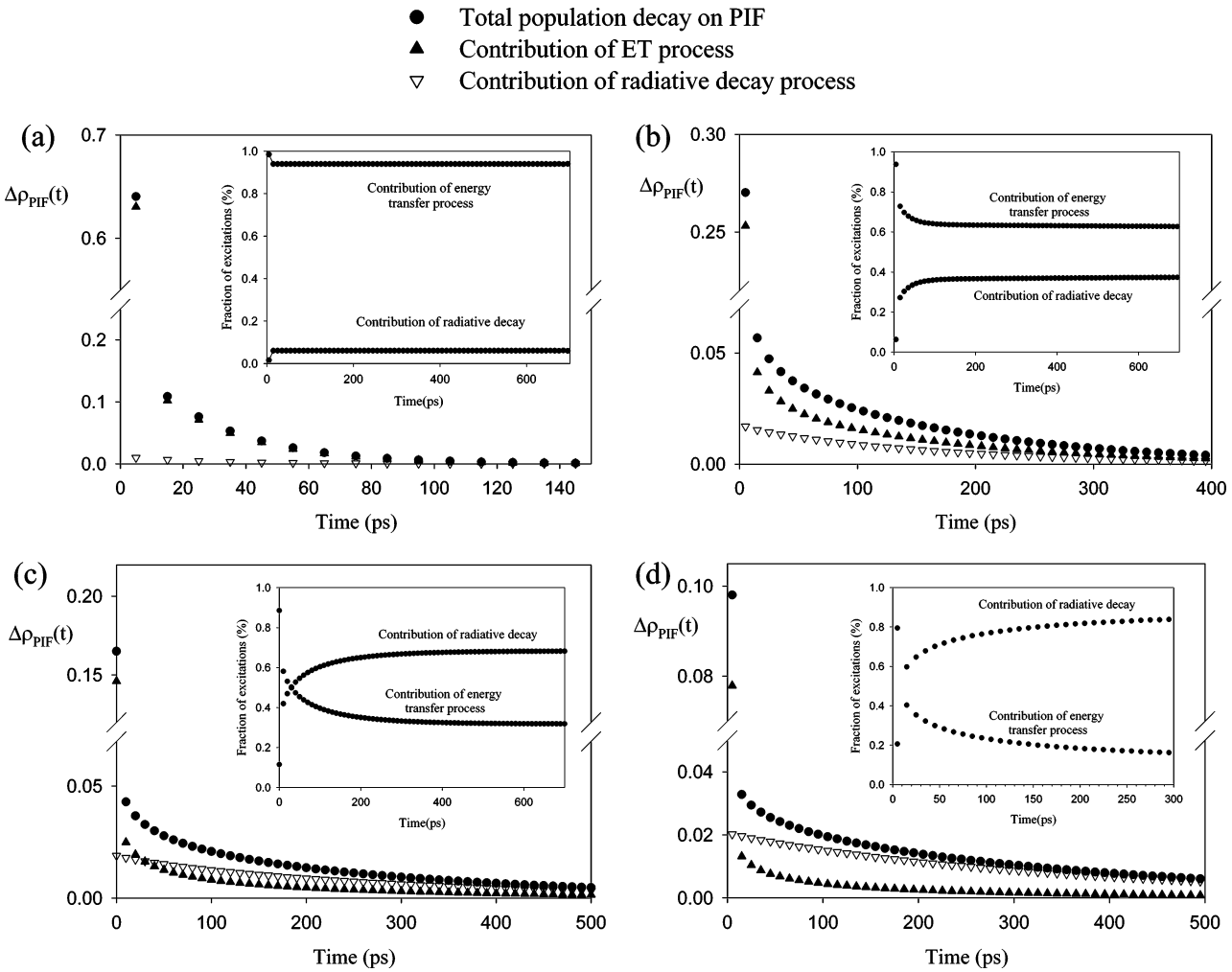

Figure 12. Time-dependent changes in PIF population within a time step of 10 ps for a total chain length of 12 (a), 30 (b), 50 (c), and 100 (d) repeat units. Individual contributions from energy transfer and radiative decay processes are also displayed. The relative efficiencies (in %) of the two competing processes are given as inset.

for chain lengths of 12, 20 and 30 units, respectively. A flat maximum spreading over the 500−700 ps time range is obtained for chain lengths of 50 and 100 indenofluorene units, the difference between the two chain lengths being mostly in terms of the total number of excitations trapped on the perylene derivative. This steady population arises from a subtle interplay between the number of excitations transferred on average from the main chain to the perylene end-groups and the number of excitations that decay radiatively on either the PIF chain or the perylene group within the same time range. The characteristic time scales for excitation motion to the perylene derivatives are indeed on the same order of magnitude as the calculated (radiative) donor excited-state lifetimes reported in Figure 7: these range from 600 to 400 ps in the more extended indenofluorene segments (from 6 to 8 repeat units). A characteristic decay time of 500 ps has been extracted from the PIF stimulated emission signal measured from time-resolved spectroscopy (see Figure 2c), which confirms that exciton propagation and decay occur on similar time scales.

The time-dependent populations on the PIF strand [ρ_{PIF} (t)], defined as the sum of excitation populations over all polymer segments, are displayed in Figure 11b for total chain lengths of 12, 20, 30, 50, and 100 units. As expected, these decay more slowly in the longer chains, a finding that is consistent with the less efficient energy transfer to the perylene endcaps. To investigate further the chain-length dependent energy-transfer efficiency, contributions from radiative and hopping processes to the PIF population decay must be disentangled. Since the backward hopping rate from the perylene derivative to the PIF chain is negligible and neglecting radiative decay on the acceptor, the increase in population on the endcap within a time step Δt provides a measure of the number of excitations that have been transferred to the chain ends within the corresponding time step.

Figure 12 shows the contributions to the overall time decay of the PIF population associated with radiative and hopping processes. The time-dependent relative efficiencies of the two decay routes (displayed in inset) are defined as:

$$\eta_{ET}(t) = \Delta\rho_{\mathrm{PIF}}^{\mathrm{ET}}(t)/\Delta\rho_{PIF}(t) \quad \text{for energy transport}$$
$$\eta_{\mathrm{RD}}(t) = \Delta\rho_{\mathrm{PIF}}^{\mathrm{RD}}(t)/\Delta\rho_{\mathrm{PIF}}(t) \quad \text{for radiative decay} \tag{20}$$

where $\Delta\rho_{\mathrm{PIF}}^{\mathrm{ET}}(t)$ and $\Delta\rho_{\mathrm{PIF}}^{\mathrm{RD}}(t)$ represent the contributions to the overall decrease in PIF population of the excitation diffusion and radiative decay processes.

The contribution to the time decay in PIF population arising from excitation transport to the perylene endcaps features an

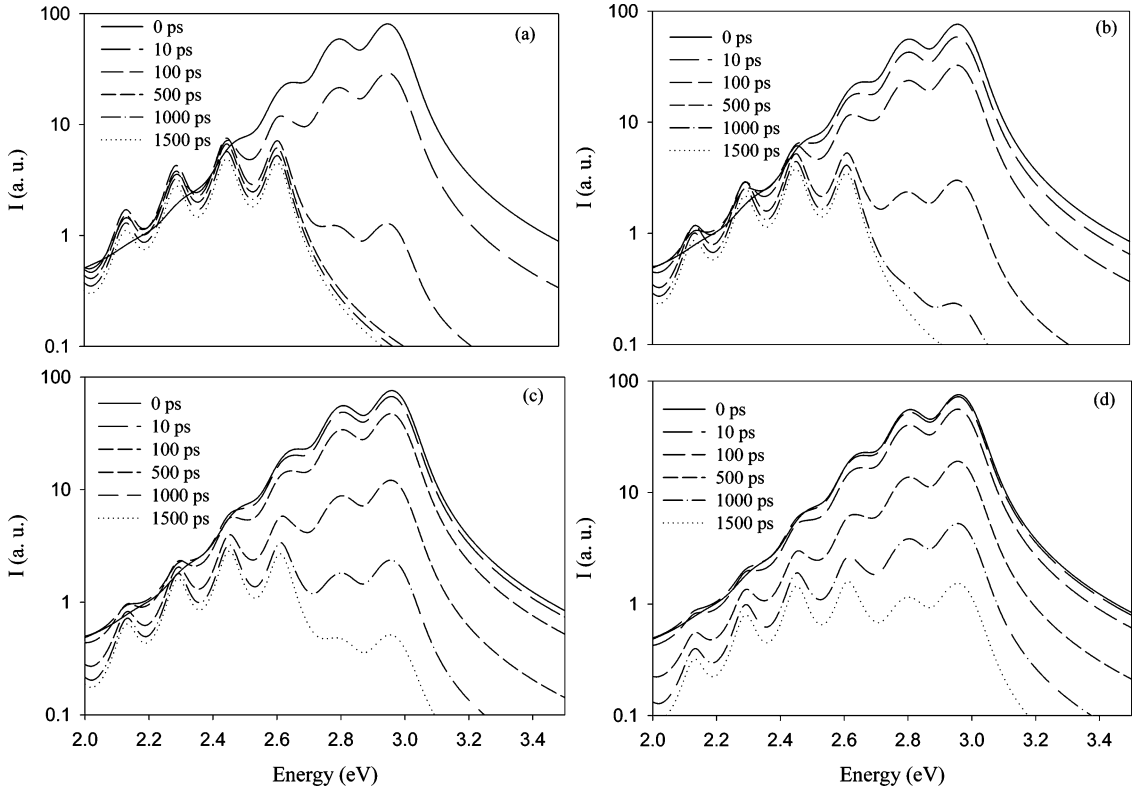

Figure 13. Time-dependent calculated emission spectra for total chain lengths of 12 (a), 30 (b), 50 (c), and 100 (d) repeat units.

initial fast decay (for instance ~60% of the excitations are transferred within the first 10 ps for $L = 12$, ~40% for $L = 20$ and ~30% for $L = 30$), followed by a slower evolution at longer time delays. This evolution can be rationalized by the slow intrachain excitation migration along the polymer backbone compared to energy transfer to the perylene end-groups from neighboring PIF segments. From the time-dependent populations on each site, one can indeed notice a fast population decay on the chromophore covalently linked to the perylene endcap within the first time steps, this site remaining poorly populated at longer time delays. Our theoretical results thus indicate that only excitations lying close to the perylene emitters can be efficiently transferred; this process then sets up the dynamics at early stage. For longer time delays, the time evolution is controlled by the repopulation rate of the chain segment adjacent to the perylene, which proceeds through migration of excitations along the polymer backbone. This clearly suggests that the time limiting step in the energy transfer to the perylene acceptor is the multistep migration along the PIF chain.

As expected, radiative decay plays a minor role in short chains including 12 and 20 indenofluorene units, where population decay on the polymer chain arises mostly from excitation diffusion. The efficiency of the energy-transfer process is found to decrease abruptly in the first 10 ps and then to level off at a limiting value of 94% and 75% for a total chain length of 12 and 20 (not shown) indenofluorene units, respectively. In contrast, both energy transfer and radiative decay processes contribute significantly for a total chain length of 30 units (Figure 12 b), where energy transport phenomena contribute about 60% to PIF population decay. Moving to chain lengths of 50 repeat units (Figure 12c) or larger, radiative decay is found to provide the largest contribution to the PIF time-dependent population decay (except at short time delays). This can be rationalized by the fact that excitations located on distant chromophores must be first brought close to the perylene groups prior to energy transfer to acceptor site. Thus, for intermediate physical chain lengths on the order of 30 indenofluorene units (i.e., close to the average chain length estimated for the system under investigation), our calculations suggest that the excitation dynamics arises from a competition between excitation motion along the polymer chain and radiative decay.

The dynamics of exciton migration in the endcapped polymer chains can also be gauged from the simulated time evolution of the photoluminescence spectra. These are shown in Figure 13 for different time delays and polymer lengths. A different picture is obtained when considering different total PIF chain lengths as a result of different ET dynamics. The time-resolved luminescence spectra computed for the shortest chain (12 repeat units) show a fast decay of PIF emission in the 0−100 ps time range, the luminescence spectrum being dominated by perylene emission for time delays larger than 100 ps. The almost stationary PEC emission then observed can be rationalized by the long radiative lifetime associated with the perylene group (~3 ns). Apart from the slower initial decay of the PIF emission, a rather similar picture is obtained for a total chain length of 20 indenofluorene units (the corresponding spectrum is not shown here).

An increasing slow-down of the PIF population decay is predicted for increasing chain lengths, which arises from inefficient transport along the polymer chains. Contributions from PIF and PEC emissions become comparable after about 500 ps, 1000 and 1500 ps for a total chain length of 30, 50, and 100 indenofluorene units, respectively. In the time-resolved experiments discussed in section IV, the polyindenofluorene chain and the perylene derivative provide comparable light emission intensities for a ~700 ps time delay. This result is

consistent with the theoretical spectra when assuming a total chain length in the range of 30−50 repeat units and a single perylene endcap per chain. Note that the time-resolved PL spectrum for a PIF chain of 70 indenofluorene units endcapped with a perylene moiety at both ends is very similar to that obtained for a singly endcapped 30-mer chain (not shown here, see complementary results). As discussed previously, these are the two most representative systems for the polymer under study. For such realistic chain lengths, the simulations lead to a decrease in PIF emission over 2 orders of magnitude over about 1 ns together with a stationary PEC emission, which are both consistent with the experimental observations. This can be rationalized in part by the rather long radiative lifetime of excitations residing on the perylene group compared to short-lived excitations lying on the PIF segments. As discussed above, both radiative decay and excitation diffusion contribute significantly to the population decay on the polymer segments, leading to the fast and important drop in the transient PIF emission signal. As the limited number of excitations reaching the perylene endcaps almost immediately decays via luminescence, the PEC emission feature shows a less pronounced time dependence that can be traced back to the flat maximum in PEC population setting up at relatively early stage of the dynamics.

VI. Conclusions

Both *intermolecular* and *intramolecular* energy-transfer processes have been assessed experimentally and theoretically in a covalently linked donor−acceptor system wherein a poly(indenofluorene) chains acting as donor are endcapped with red-emitting perylene derivatives. Contributions of *interchain* and *intrachain* processes to the overall energy-transfer process have been determined by recording time-resolved photoluminescence and absorption spectra of the system under investigation in both solution and thin film. In solution, the energy-transfer process occurs on a 500-ps time scale and competes with radiative/nonradiative decay of the excitations. Energy transfer is found to be much more efficient (a few tens of picoseconds) in the solid state leading to a complete quenching of the polyindenofluorene luminescence. This difference in dynamical behavior is to be related to the emergence of additional channels for the excitation migration in films as a result of the presence of close contacts between adjacent chains.

To rationalize the different dynamics observed in solution and in the solid state, we have described intramolecular and intermolecular transfer processes by means of models with an increasing level of sophistication. Intramolecular energy-transfer processes along the polymer main chain have been described first by using a simple model wherein only hopping to the nearest neighbors has been considered, therefore providing an upper limit to the actual rate of excitation energy motion. Electronic couplings, spectral overlaps, and energy-transfer rates have been computed in the framework of an improved Förster model based on a multicentric monopole representation of the transition electronic densities, for several donor/acceptor pairs, differing by the size of the indenofluorene segments involved. We find that the electronic couplings and the corresponding transfer rates for intrachain energy migration drop quickly with the size of the donor and acceptor groups. This can be ascribed to the increased inter-site separations, together with a concomitant decrease in transition density at the edge of the conformational subunits. The same trend is observed when considering the rate of energy transfer between oligoindenofluorene segments with various conjugation lengths and the perylene group as the final acceptor. Compared to exciton motion along the conjugated chains, energy transfer from an indenofluorene segment to an attached perylene derivative is calculated to be typically 2 orders of magnitude faster. Such a significant difference in transfer rates stems from higher electronic couplings for intrachain heteromolecular transfer with respect to homomolecular hopping and also more efficient donor−acceptor overlap in the former case. Small spectral overlaps for intrachain hopping between OIF conjugated segments result from the large relaxation energy associated mostly with the pronounced changes in conformation when going from the (twisted) ground-state to the (planar) excited-state geometries. Thus, in situations where intermolecular processes are unlikely, the determining step for energy transfer to the endcapping perylene corresponds to the slowest hopping process along the conjugated main chains.

Interchain energy transfer in the homopolymer has then been modeled by considering the case of two interacting poly(indenofluorene) chains packed in a cofacial arrangement. The electronic couplings and the corresponding transfer rates computed for different OIF_n/OIF_m complexes differing by the size of the conjugated segments in interaction, are always found to be larger than the corresponding intrachain values. The same behavior is observed for complexes formed by a perylene derivative lying on the top of oligoindenofluorene segments. According to these results, close contacts between molecules provide an efficient pathway for energy migration in conjugated materials as a result of increased donor−acceptor electronic couplings. That *interchain* exciton migration is faster than *intrachain* migration is consistent with the increase in transfer rate observed experimentally when going from solution to the solid state. It should be borne in mind, however, that the rates of intrachain processes would increase significantly if the chains were perfectly conjugated and the excitations coupled coherently along the chains.

Long-range intrachain energy transfer, namely light harvesting and trapping of the excitation, has been modeled based on the hopping rates calculated using the improved Förster model. A set of Pauli master equations for exciton migration has been solved considering random chains built from a distribution of conjugated segments with various lengths. The dependence of the transfer dynamics on the total chain length as well as on the typical length and distribution of the conformational subunits has been studied. We find that the overall transfer process is faster in polymer chains built from short conjugated segments as a result of an increase in the site-to-site electronic coupling leading to faster exciton hops. As expected, the characteristic time for energy transfer increases with chain length, while the number of excitations effectively reaching the perylene group decreases.

From a detailed analysis of the various contributions to the population decay, we have found that the dynamics results from a competition between radiative decay over PIF segments and energy-transfer processes along the chains for physical lengths in the order of 30 indenofluorene units (i.e., in the range of the actual average chain length of the polymer under study). Our results suggest that a fast initial hopping process takes place to the perylene from the covalently attached indenofluorene

chromophore; this is then followed by slow migration among conjugated segments along the main polymer backbone, which is the time-limiting step in the overall energy transfer to the perylene endcaps.

Transient photoluminescence spectra have also been simulated on the basis of the time-dependent populations for different time delays and polymer lengths. These PL spectra indicate a slower decay of the PIF emission signal with increasing chain length as a result of less efficient overall excitation migration toward the endcaps. In all cases, a decrease of the PIF emission over 2 orders of magnitude together with a stationary PEC emission are found. Both features are consistent with the experimental results and result from a subtle balance between radiative decay on the PIF segments and PEC acceptors and excitation hopping process along the polymer chains. In particular, the theoretical spectra obtained for a total chain length of 30 units, assuming mono endcapped molecules, agree well with experimental results, with equal contributions from PIF and PEC emissions achieved for a 500 ps time delay.

Acknowledgment. The work in Mons is partly supported by the Belgian Federal Government "InterUniversity Attraction Pole in Supramolecular Chemistry and Catalysis (PAI 4/11)" and the Belgian National Fund for Scientific Research (FNRS-FRFC). E.H. and D.B. are research fellow and research associate of the Belgian National Fund for Scientific Research (FNRS), respectively. The work at Georgia Tech is partly supported by the National Science Foundation (CHE-0342321 and the STC Program under Award Number D.M.R.-0120967), the Office of Naval Research, and the IBM SUR Program. G.D.S. thanks the Natural Sciences and Engineering Research Council of Canada for financial support. The work in Cambridge is supported by a grant from the UK Engineering and Physical Sciences Research Council (EPSRC); C.S. acknowledges further support from the EPSRC via an Advanced Research Fellowship. L.M.H. would like to thank St. John's College Cambridge for support through a Research Fellowship. The Cambridge-Mons collaboration is supported by the European Commission (LAMINATE).

Supporting Information Available: Derivation of eq 2 for hopping rates, figures of spectra, figures of electronic couplings. This material is available free of charge via the Internet at http://pubs.acs.org. [a]The PR values refer to repeat units.

JA0488784